

AD-A034 939

AIR FORCE INST OF TECH WRIGHT-PATTERSON AFB OHIO SCH--ETC F/6 19/4
BALLISTIC IMPACT BETWEEN A BLUNT ELASTIC PROJECTILE AND AN ELAS--ETC(U)
DEC 76 K C LEONE

UNCLASSIFIED

GAE/MC/76D-4

NL

[OF]

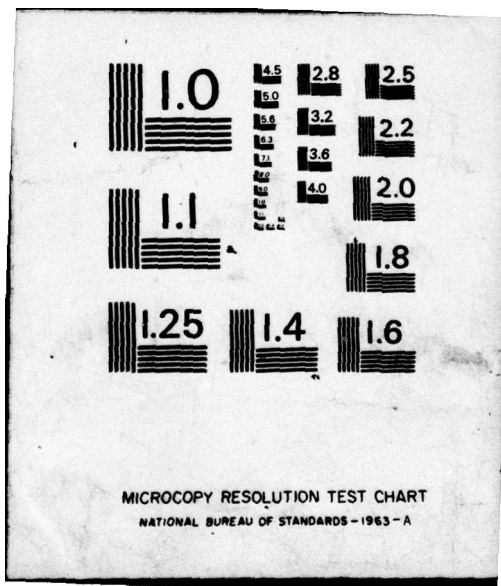
AD
A034939

12



END

DATE
FILMED
3-77



1

D D C
DEC 28 1977
RECEIVED

6

BALLISTIC IMPACT BETWEEN A BLUNT
ELASTIC PROJECTILE AND AN
ELASTIC-PLASTIC PLATE.

11 Dec 76

THESIS

10

14

GAE/MC/76D-4

Kenneth C. Leone
Captain USAF

12 78p.

9 Master's thesis

Approved for public release; distribution unlimited.

012225

4B

**BALLISTIC IMPACT BETWEEN A BLUNT
ELASTIC PROJECTILE AND AN
ELASTIC-PLASTIC PLATE**

THESIS

**Presented to the Faculty of the School of Engineering
of the Air Force Institute of Technology
Air University
in Partial Fulfillment of the
Requirements for the Degree of
Master of Science**

by

**Kenneth C. Leone
Captain USAF**

Graduate Aeronautical Engineering

December 1976

Approved for public release; distribution unlimited.

PTIS	White Section	<input checked="" type="checkbox"/>
SEARCHED	Red Section	<input type="checkbox"/>
INDEXED		<input type="checkbox"/>
BY DISTRIBUTION/AVAILABILITY CODES		
Dist.	Avail.	or SPECIAL
A		

Preface

This study is my attempt to model the blunt projectile impact problem. I have extended a model developed by my thesis advisor, Capt. Richard D. Binkowski. His important analytical finding, that the elastic wave action is of primary importance in the plugging failure mechanism, provided the impetus for an elastic/elastic-plastic wave model. I have attempted to develop such a model in order to provide more accurate initial conditions for use in further analytical studies and in experimental impact work.

I would like to thank Capt. Binkowski for his enthusiastic presentation of this thesis topic early in my academic program. This enabled me to plan course work that provided background in impact phenomena. He also provided the excellent guidance needed to keep an analytical study from wandering into diverse areas.

I would like to thank Dr. Peter J. Torvik for valuable course guidance that not only provided background for my thesis, but also enriched my academic program by exposing me to new and challenging concepts.

I would like to thank Dr. Anthony N. Palazotto for an excellent foundation in elasticity and for his personal encouragement.

I would like to thank Mrs. Barbara Barnes for providing excellent typing service under difficult conditions.

I wish to especially thank my wife, Mary Ann, for providing an atmosphere that made a personal challenge a rewarding family experience.

Contents

Preface	ii
List of Figures	v
Abstract	viii
I. Introduction	1
Background	1
Purpose	3
Approach	3
Scope	4
II. Development of Model	6
Geometry	6
Stress Wave Properties	10
Stress Wave Interactions	15
Optimum Conditions	27
III. Results	29
Introduction	29
Discussion	29
IV. Application to Plate Impact	40
Introduction	40
Failure Criteria	40
Discussion	41
V. Recommendations	46
Bibliography	47
Appendix A: Initial Impact Solution	48
Appendix B: Initial Elastic-Plastic Wave Interaction	51
Appendix C: Plastic-Unloading Wave Interaction	55
Appendix D: Critical (T/L) Solutions	59
Analytical	59
Graphical	62

List of Figures

Figure		Page
1	Deformation and Failure Mechanisms for Plate Deformation	2
2	Initial Impact Geometry	7
3	Basic Dimensions	8
4	Graphical Wave Interaction Presentation .	9
5	Wave Front Particle Velocity Relationships	11
6	Constitutive Relations	12
7	Initial Impact Wave Relationships	13
8	Initial Elastic-Plastic Wave Interaction and Optimum T/L	16
9	Two Cases of Initial Elastic-Plastic Interaction	17
10	Successive Elastic-Plastic Interactions .	20
11	Interference of Elastic Wave From Projectile ($T/L > 1$)	22
12	Plastic-Unloading Wave Interaction . . .	23
13	Elastic Wave Interaction With Reduced Plastic Wave	24
14	Simultaneous Interaction of the Three Initial Waves	26
15	V_0 vs. (T/L)	30
16	(T/L) Shift on Third Sub-impact	34
17	Delayed Plastic Wave Initiation on Second Sub-impact	35
18	Comparison of Average Velocities at Separation for Free Rod Impact	38
19	Comparison With Experimental Failure Data	44

Figure		Page
A-1	Initial Impact Wave Relationships	48
B-1	Initial Elastic-Plastic Wave Interaction	51
C-1	Plastic-Unloading Wave Interaction	55
D-1	Analytic Solution for T/L Critical	59
D-2	Graphical Solution for T/L Critical	63

Nomenclature

A	Slope of Plastic Stress—Strain Curve in Tension
B _e	Elastic Wave Velocity
B _p	Plastic Compressive Wave Velocity
\bar{B}	$\frac{B_p}{B_e}$
B	Plastic Shear Wave Velocity
C	General Wave Speed
d	Projectile Diameter
F _s	Shear Force at Periphery of m
k	Unimpacted Plate Shear Yield Stress
L	Projectile Length
M	Projectile Mass
\bar{M}	Mass Ratio $\bar{M} = m/M$
m	Plate Mass Beneath Projectile
T	Plate Thickness
t	Time Variable
V ₀	Initial Projectile Velocity
v	General Particle Velocity Behind Stress Wave
V _a	Average Particle Velocity Imparted to Plug
γ	Shear Strain on Periphery of Plug
ρ	Material Density
τ	Shear Stress
σ _y	Tensile Yield Stress
σ	General Stress Behind Stress Wave

Abstract

A cylindrical rod on rod impact model is developed that allows for linear elastic strains in the projectile and linear elastic-plastic strains in the target plug. Application is made to the plate impact problem. Normal incidence impact of two circular cylinders is considered. One-dimensional stress waves load the projectile and the plug in compression and tension. Stress wave interactions are tracked in the projectile and in the plug. Momentum balance is used to solve for resultant stresses and particle velocities. Optimum conditions are determined for the initial impact that allow the plug to be accelerated uniformly to the initial projectile velocity. Optimum plug length/projectile length ratio is found to decrease with increasing projectile initial velocity. Separation of the projectile and plug is predicted and separation times are determined. Average velocities at separation are determined and plotted vs. plug length/projectile length ratio. A comparison is made on this plot with the elastic/elastic and the rigid/elastic free rod cases. A velocity reversal region is identified, where the average projectile velocity is greater than the average plug velocity at separation, which causes the free rods to reimpact. The model provides an initial condition for the plate impact problem. The optimum plate thickness/projectile length ratio increases on subsequent

sub-impacts. Qualitative extensions indicate optimum plugging conditions. The model suggests that for thin plates the plate material is accelerated to the initial projectile velocity. It also suggests that projectiles are essentially rigid for thick plate impacts as long as the projectile does not deform plastically.

BALLISTIC IMPACT BETWEEN A BLUNT
ELASTIC PROJECTILE AND AN
ELASTIC-PLASTIC PLATE

I. Introduction

Background

The Air Force is interested in impact from the standpoint of projectile and armor plate design. The general design criteria is to cause or prevent failure of a plate-like structure. In order to design material and geometric properties for either of these conditions, it is necessary to understand the mechanism of plate failure.

Analytical studies have shown that a principle factor in the failure mechanism is the method by which momentum is transferred from the projectile to the plate. The accuracy, and the value, of an analytical model depends on how the momentum transfer is modeled. In order to obtain a workable mathematical model, it is generally assumed that penetration and failure occur predominately by a single mechanism with the effect of others being negligible. The three primary mechanisms are shown in Fig. 1, with the plugging mode being of primary interest in this analysis.

Previous data on plugging failure have been essentially empirical and have been focused on either the determination

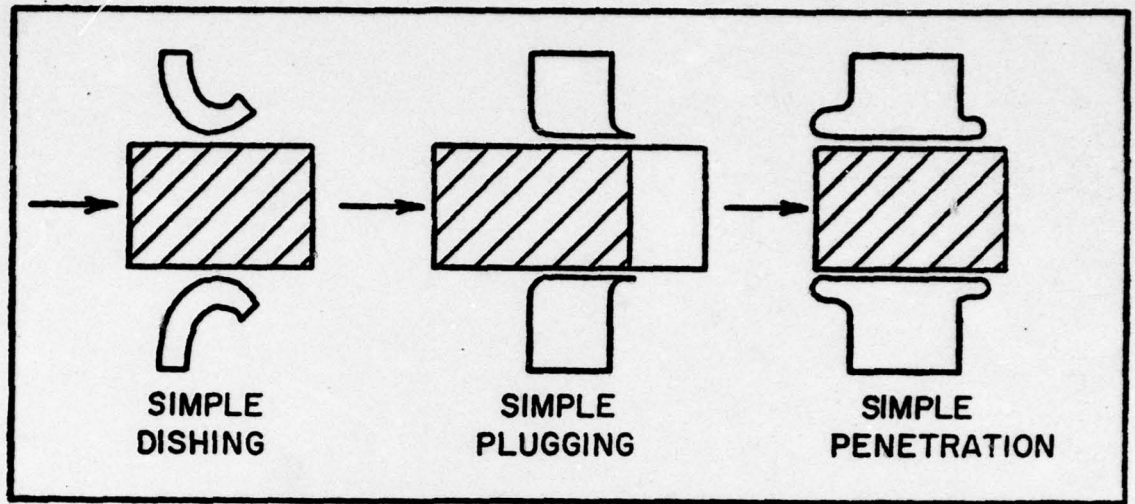


Figure 1. Deformation and Failure Mechanisms for Plate Perforation (From Ref. 1)

of the minimum velocity required for penetration or on plate plastic deformation. Most of the plugging models assume that the plastic deformation is of primary interest and that the projectile and plate remain in contact during a continuous failure process. These models pay little attention to the manner by which the plate material beneath the projectile is accelerated.

In contrast with the previous models, Binkowski (Ref 1) has shown that plate failure criteria is critically dependent on the value of this initial condition. Rather than neglecting the elastic compressive/tensile waves which result from the impact, he based the initial velocity condition on their action. This elastic wave modeling significantly alters the predicted impact process. In particular,

it predicts separation of the projectile and plate upon return of the reflected elastic wave so that most of the outer plate deformation occurs with the plate and projectile separated. After the plate material is decelerated by outer plate deformation, it is reimpacted by the projectile and reaccelerated. This sequencing of reimpacts results in highly localized shear deformation. The model gives good results, and fills an analytical gap in predicting impact failures. As with any new theory or concept, its real value comes when its extension or application results in deeper insight into the basic mechanisms of a complex process.

Purpose

The purpose of this analysis is to extend the above model for plate material acceleration. Binkowski considered a rigid projectile and neglected compressive plastic strains. The present analysis considers an elastic projectile impacting a linear work-hardened plug, i.e., an elastic/elastic-plastic impact. It treats the plug as a free cylinder during the acceleration process and therefore provides initial velocity conditions for the problem of an accelerated plug imbedded in an otherwise initially stationary plate.

Approach

This study is entirely analytical. One-dimensional finite amplitude stress wave theory is applied to both the

elastic projectile and the elastic-plastic plug.

The stress in the plug loads elastically and plastically in accordance with a linear work-hardening, strain rate independent, constitutive relation. It unloads elastically in a strain rate independent manner. The stress in the hardened projectile loads and unloads elastically over the entire stress range.

Conservation of momentum is used to solve for the stresses and particle velocities after the initial impact and after each internal wave interaction.

Separation of the projectile and plug occurs when a net tensile stress state is present at the interface. Average particle velocities for the projectile and plug are calculated for the time of separation. Optimum initial velocities and geometric conditions (plate thickness/projectile length ratio) are determined by identifying optimum plug acceleration conditions.

The process is modeled as a cylindrical rod on rod impact. This constrains all the momentum transferred from the cylindrical projectile to the plate mass plug beneath it.

Scope

1. The impact and response are axisymmetric.
2. The impact occurs at normal incidence.
3. The projectile is a hardened elastic circular cylinder.

4. Only the first sub-impact is considered. Qualitative extensions are made for the complete impact process.

5. The study is limited to the case of the projectile and plate being the same material. For the purpose of specific calculations, the plug material is 230 Brinell Hardness steel. Wave speeds are calculated from experimentally measured data (Ref 2).

6. A comparison is made with rigid and elastic models for the impact of two free cylinders.

7. The model is of a free cylinder on free cylinder impact. As such it is an approximation to plate impact which neglects deceleration of the plug mass due to radial wave action while it is being accelerated by the projectile. The simplification does, however, add clarity to interpretation of the results. It also supplies predicted initial conditions which are valid whenever the time to accelerate the plug is short compared with total plate deformation time. This situation is shown to exist when the geometry is favorable for plugging type failures (Ref 1).

II. Development of Model

Geometry

The interaction between the projectile and the plate is modeled as the impact between two blunt circular cylinders. The geometry is shown in Fig. 2 where F_s is the shear force acting on the plug due to the outer plate material. The basic dimensions and coordinate system are shown in Fig. 3. The elastic circular cylinder has mass M , length L , and density ρ . The initial velocity of the projectile is V_0 . All compressive and tensile waves in the plate are constrained within the plug and the wave motion is along the z -axis. Shear waves move out radially from the periphery of the plug. The time of contact is assumed very short which restricts momentum transfer to the immediate region of the plug periphery. The plate is assumed large enough that the radial shear waves do not reflect from the edges of the plate. The elastic and plastic waves within the plug, however, do reflect from the free end of the projectile and the plug causing wave interactions.

Due to the complexity of the wave interactions, a graphical method of tracking the wave locations is useful. Fig. 4 shows the basic time-distance plot used to track wave locations.

The angles α_e and α_p are proportional to $\tan^{-1} \frac{1}{B_e}$ and $\tan^{-1} \frac{1}{B_p}$ respectively. The location of any wave front is specified at any given time. As shown in Fig. 4, the

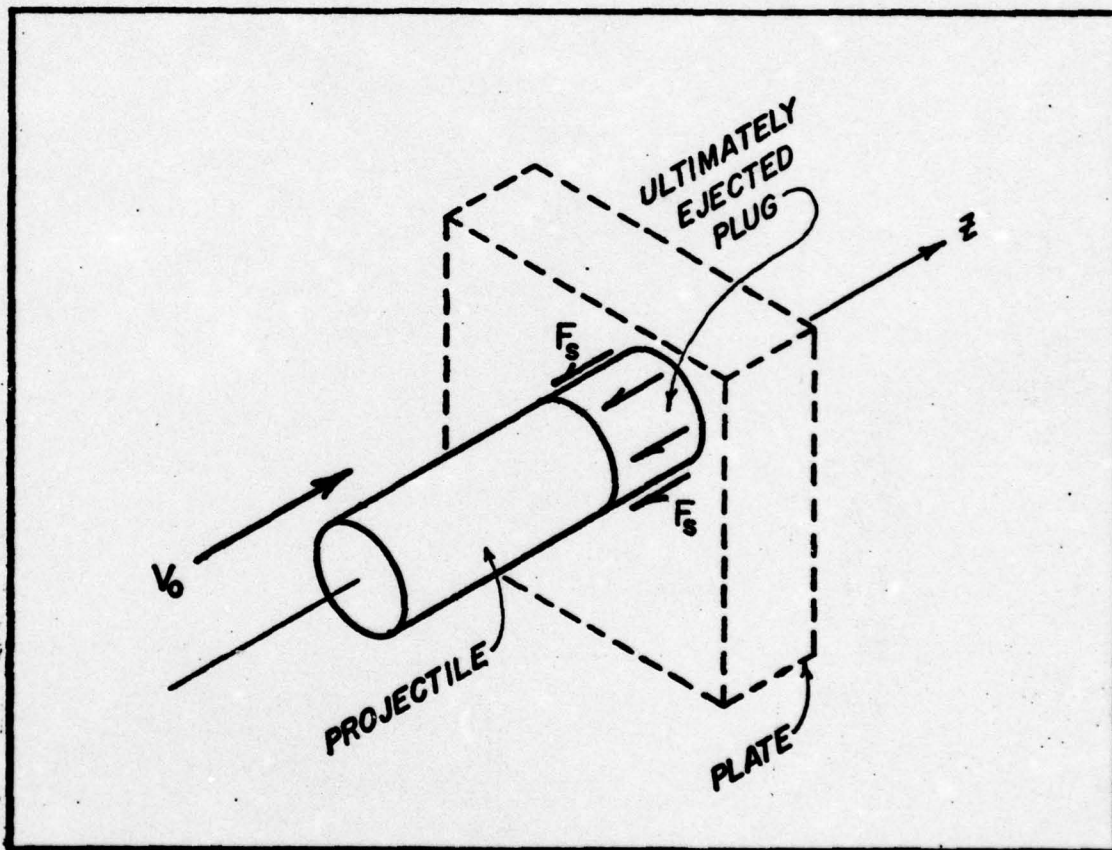


Figure 2. Initial Impact Geometry

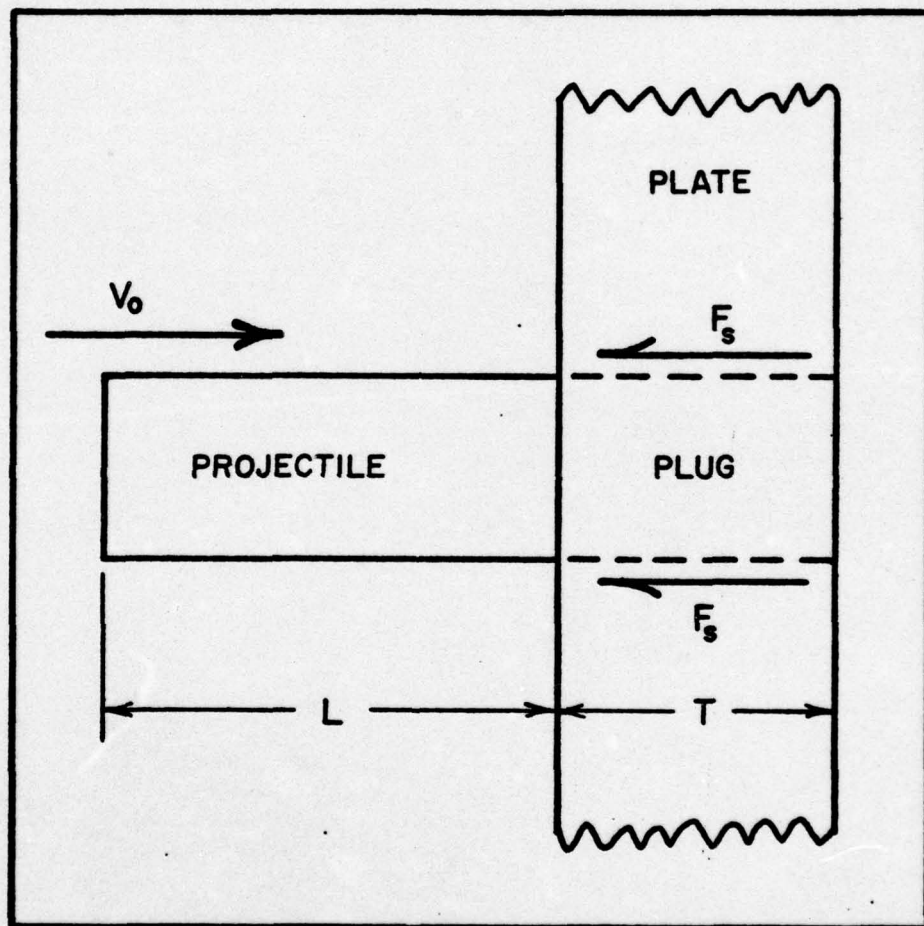


Figure 3. Basic Dimensions

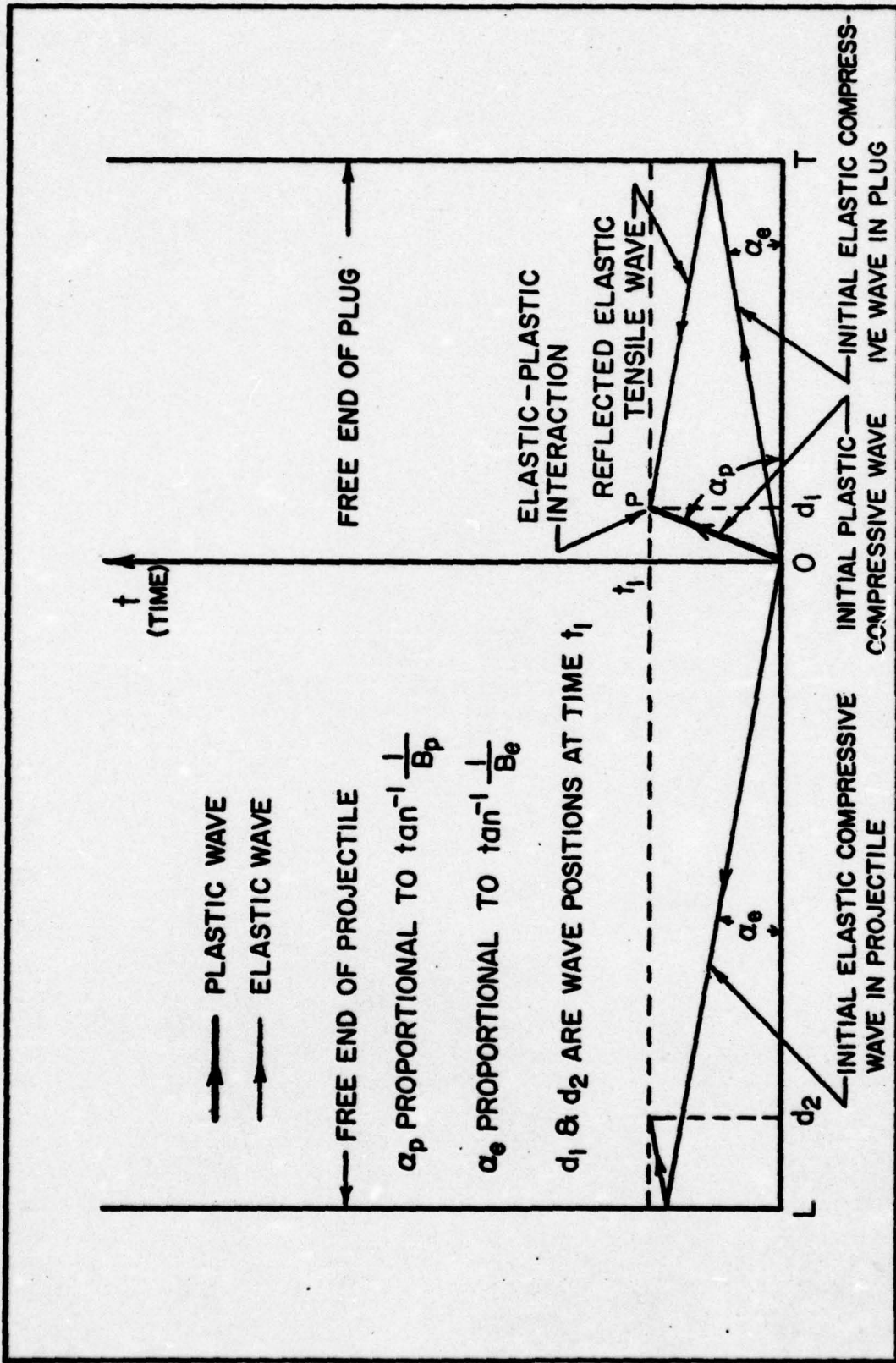


Figure 4. Graphical Wave Interaction Presentation

reflected elastic wave in the plug interacts with the plastic wave at point P. This interaction occurs at time t_1 and at a distance d_1 into the plug. At the same time the elastic wave in the projectile is located a distance d_2 in the projectile. The distances T and L do not have to be actual distances as long as the T/L ratio is the same as the desired interaction. In this case the distances d_1 and d_2 are percentage distances. The reference system is coincident with the moving interface and is material fixed. Due to the obvious dependence of wave interaction locations on the T/L ratio, this diagram is used extensively to keep track of specific wave interactions as well as to graphically solve for specific T/L ratios that will allow critical wave interactions to take place.

Stress Wave Properties

Discontinuous stress waves move through materials at characteristic wave velocities. Both stress jumps and particle velocity jumps occur at the wave fronts. The magnitude of the stress jump is given by the momentum balance across the wave. The basic stress jump condition is

$$\Delta\sigma = -\rho C\Delta v \quad (1)$$

where C is the wave velocity for the particular wave, $\Delta\sigma$ is the stress jump across the wave, Δv is the particle velocity jump across the wave, and ρ is the initial material density. Since the final stress behind the wave is of

primary interest, the jump equation is put in the more convenient form;

$$\sigma_{\text{final}} = \sigma_{\text{initial}} - \rho C(v_{\text{final}} - v_{\text{initial}}) \quad (2)$$

When a coordinate system is established, the appropriate sign is given to the wave velocity and the particle velocities. Equation (2) is used for all of the one-dimensional wave interactions along the z-axis.

Compressive waves impart particle velocity jumps in the same direction as the wave motion. Tensile waves impart particle velocity jumps in the opposite direction of the wave motion. Where the compressive and tensile waves meet the periphery of the plug the stress is assumed to jump from a state of pure compression to a state of pure shear. The shear wave front moves in the radial direction but imparts a particle velocity parallel to the wave front or in the positive z-direction. The relationships of particle velocity to wave front motion is shown in Fig. 5.

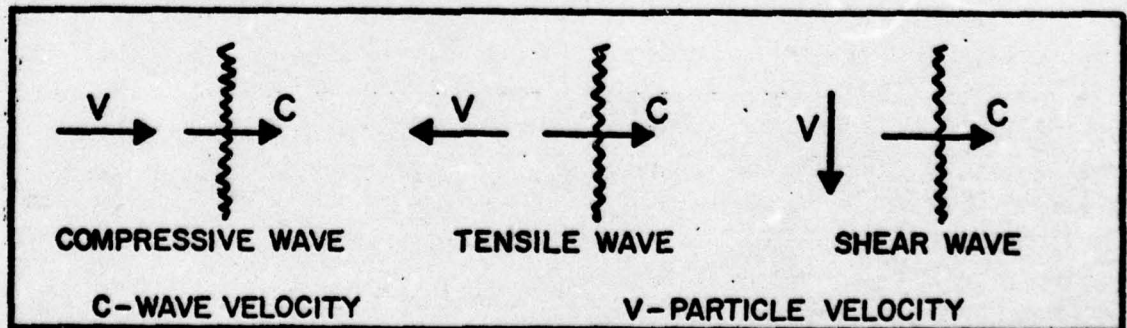


Figure 5. Wave Front Particle Velocity Relationships

The Von-misses yield criteria is used to relate the compressive yield point to the shear yield point by the relationship

$$k = \sigma_y / \sqrt{3}$$

where k is the shear yield stress and σ_y is the tensile/compressive yield stress (Ref 3:70). Elastic-plastic tensile loading is shown by Fig. 6. It is assumed that both states of stress have the same octahedral shear stress-strain relation. The plug material is assumed to stress load in plastic compression according to Fig. 6a.

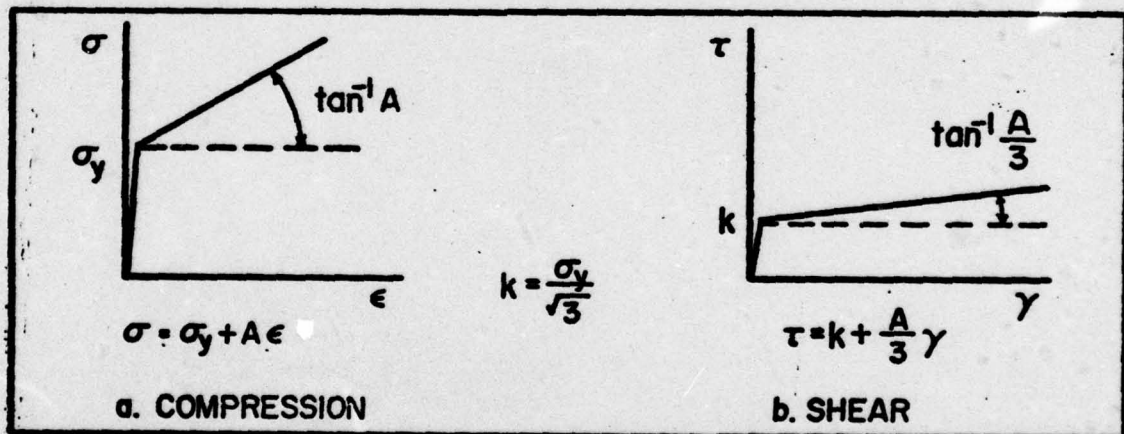


Figure 6. Constitutive Relations

If a material is impacted with an initial velocity sufficient to cause a compressive stress, σ_1 , above the yield point, two stress waves are generated as shown in Fig. 7. An elastic precursor wave travels through the

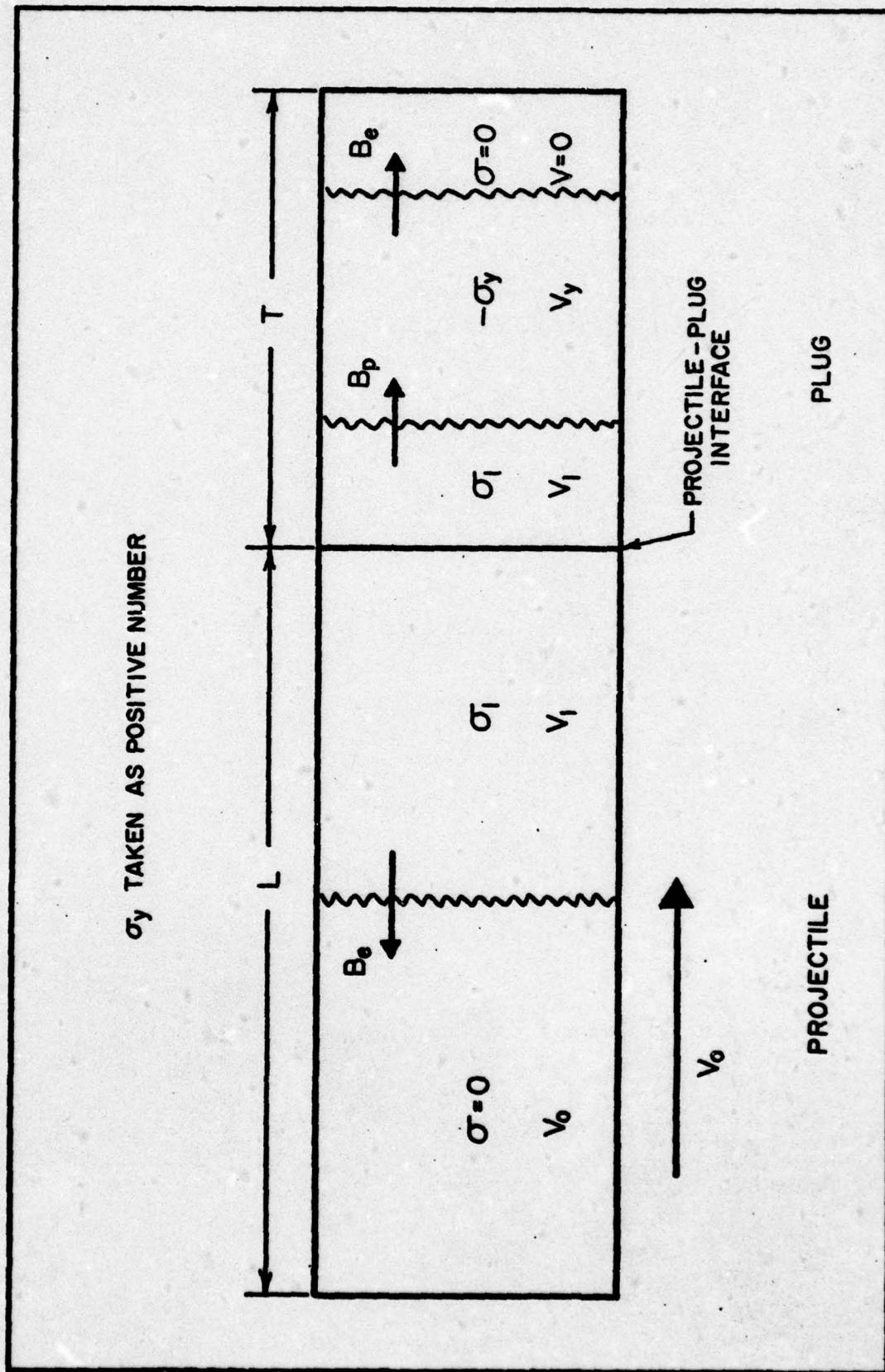


Figure 7. Initial Impact Wave Relationships

material at the elastic wave velocity given by

$$B_e = \sqrt{\frac{E}{\rho}}$$

The elastic wave results in a compressive stress, at the yield point, behind it and a particle velocity, V_y , which is calculated using equation (2). The slower plastic wave travels through the material at the plastic wave velocity which is given by

$$B_p = \sqrt{\frac{A}{\rho}}$$

where A is the slope of the plastic compressive stress curve shown in Fig. 6a. The plastic wave increases the magnitude of the stress from $-\sigma_y$ to σ_1 and increases the particle velocity from V_y to V_1 (Ref 4). Since the model being studied has finite dimensions, the effect of stress wave reflections and interactions is considered.

Before internal wave interactions take place in both the projectile and plate, the initial impact conditions must be determined. The initial impact wave geometry is shown in Fig. 7. Initial impact velocity for the projectile is V_0 . It is assumed that the impact causes a stress, σ_1 , above the yield strength. If this is not the case, the process reduces to an elastic impact which is solved for the minimum V_0 required to produce an initial plastic wave. In the plug, an elastic wave at the yield value is

followed by a plastic wave at a stress of σ_1 . In the projectile, an elastic wave with a stress of σ_1 travels to the left. Since the stress must be the same on both sides of the interface, equation (2) is used to solve for σ_1 and V_1 as shown in Appendix A. The stress jump equations become

$$\sigma_1 = -\rho B_e (V_0 - V_1)$$

on the left of the interface, and

$$\sigma_1 = -\rho B_e V_y - \rho B_p (V_1 - V_y)$$

on the right. These are solved yielding

$$V_1 = \frac{V_0 - V_y(1 - \bar{B})}{(1 + \bar{B})} \quad (3)$$

and

$$\sigma_1 = \frac{-[\rho B_p V_0 + \sigma_y(1 - \bar{B})]}{(1 + \bar{B})} \quad (4)$$

where $\bar{B} = \frac{B_p}{B_e}$. With V_1 and σ_1 known the first important stress wave interaction is solved.

Stress Wave Interactions

For relatively short plugs, the first important wave interaction takes place when the initial elastic compressive wave reflects from the free end of the plate as a tensile wave and interacts with the initial plastic compressive wave in the plug. Figure 8 shows this interaction

graphically at point P_1 .

The projectile is assumed long enough that the reflected tensile wave does not enter the plug before the interaction takes place. The interference condition is worked later. Fig. 8 is used to construct Fig. 9 which depicts the conditions before and after the interaction. The point of the wave interaction is treated as an internal interface across which the stresses and particle velocities must be equal. This enables equation (2) to be used to solve for the stresses and particle velocities resulting from all similar interactions.

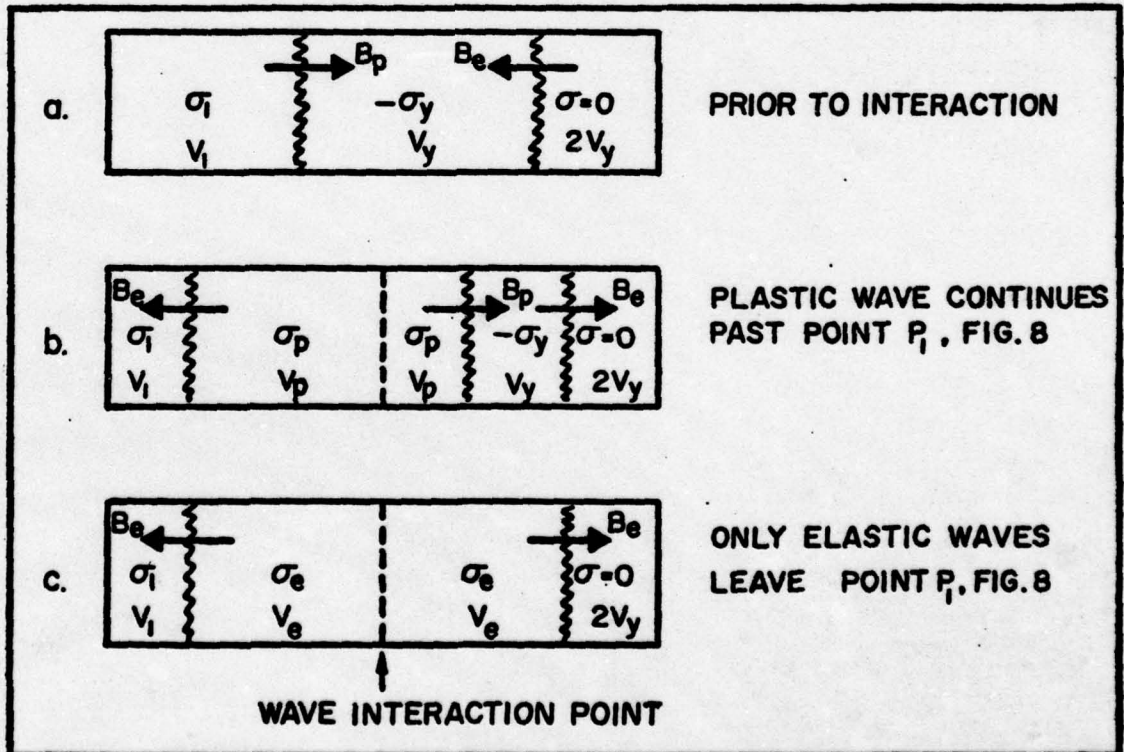


Figure 9. Two Cases of Initial Elastic-Plastic Interaction

Figures 9b and 9c show the two possible conditions that can exist after the interaction. Either an additional plastic wave of reduced magnitude leaves the interaction with an elastic wave at the yield point in front of it or the initial plastic wave is reduced below the yield point and only an elastic wave below the yield point continues into the plug. Since the initial velocity, V_0 , is the only variable in the resulting equations, regions for additional plastic wave action or only elastic wave action are found. The boundary value of V_0 is found by taking the case in Fig. 9c and setting the resulting stress equal to $(-\sigma_y)$ as a limiting elastic case just prior to producing an additional plastic wave. V_0 can also be solved for using the case in Fig. 9b.

As shown in Appendix B, the stress and particle velocity in Fig. 9b are solved for yielding

$$V_p = \frac{V_0 - V_y(1 - 3\bar{B})}{(1 + \bar{B})} \quad (5)$$

and

$$\sigma_p = -\rho B_e \left(\frac{V_0 \bar{B} + V_y(1 - 3\bar{B})}{(1 + \bar{B})} \right) \quad (6)$$

where $\bar{B} = \frac{B_p}{B_e}$.

The stress and particle velocity in Fig. 9c are solved for, yielding

$$V_e = 1/2V_0 + V_y \quad (7)$$

and

$$\sigma_e = -\rho B_e(1/2V_o - V_y) \quad (8)$$

When $\sigma_e = -\sigma_y$ the region for a second plastic wave is found to be

$$V_o > 4V_y \quad (9)$$

When the limiting velocity condition is applied to the previously mentioned initial waves, the velocity region that will give an initial plastic wave is found to be

$$V_o > 2V_y \quad (10)$$

In either case, a tensile wave returns to the interface that reduces the stress, but does not reduce it to zero. This method is applied to each successive elastic-plastic interaction as shown in Fig. 10. Subsequent regions for the initial velocity to yield additional plastic waves are found. It is assumed that the projectile is long enough that the elastic wave in the projectile does not interfere with the elastic-plastic interaction in the plug.

When the elastic wave in the projectile does return to the interface it results in a zero stress state behind it. This elastic wave passes through the interface bringing the interface stress to zero, but does not cause separation of the projectile and plug. This is shown in Fig.

11. The elastic wave catches the initial plastic wave in the plug at point P prior to point P₁ in Fig. 11, if the T/L ratio is large enough. When this happens the interaction is the same as a relaxation or unloading wave overtaking a plastic wave front. This condition also exists when separation takes place. Since unloading takes place elastically along a line parallel to the elastic stress-strain curve, the unloading wave travels at the elastic wave velocity and catches the plastic wave front. In this case, the unloading wave can reduce the plastic wave front below the elastic limit. This would eliminate additional elastic reflections and interfere with optimum momentum transfer. When a reduced plastic wave continues past the unloading interaction, a compressive elastic wave returns to the interface as shown in Fig. 12 (Ref 5:172). Each time this compressive wave returns through the interface to the projectile rear surface it reflects as a tensile unloading wave and reduces the plastic wave. These successive unloading interactions only occur for large T/L, which is beyond the primary plugging region of interest in this analysis. For 230 BHN steel, this is $T/L > 1.146$. The value of σ_2 in Fig. 11 and the corresponding V_2 are found using equation (2) as shown in Appendix C.

When the resulting plastic wave from point P in Fig. 11 interacts with the initial elastic wave at point P₁ in Fig. 11, a third important wave interaction takes

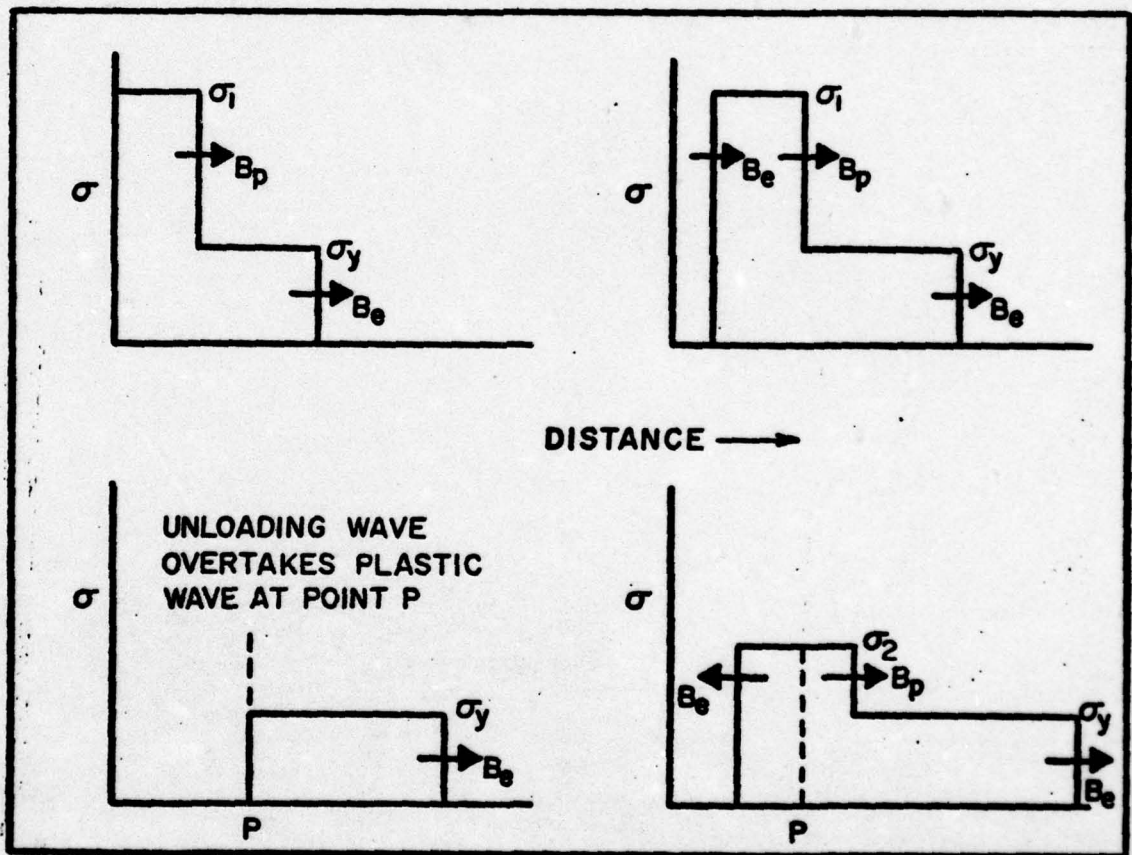


Figure 12. Plastic-Unloading Wave Interaction With Resultant Plastic Wave (From Ref 5:172)

place. This is similar to the first elastic-plastic interaction except the stress behind the plastic wavefront is lower. It is also possible to find regions of V_0 for this condition that allow an additional plastic wave to leave point P_1 in Fig. 11. The conditions prior to and after the interaction are shown in Fig. 13 for the case when the additional plastic wave is not produced. This is the case that allows the easiest solution for the V_0 regions. The stress equations using equation (2) on both

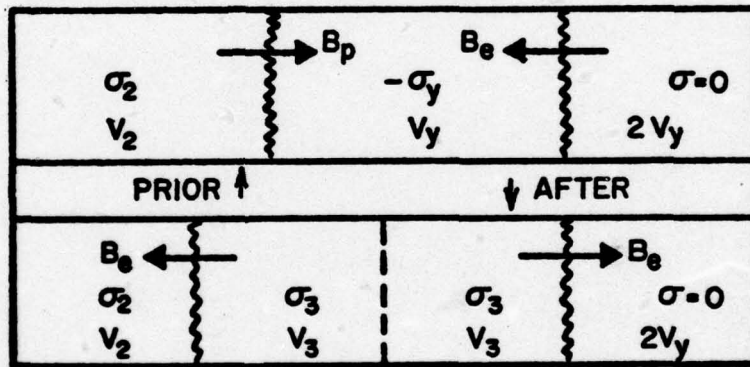


Figure 13. Elastic Interaction with Reduced Plastic Wave

sides of the interface are

$$\sigma_3 = \sigma_2 + \rho B_e (V_3 - V_2)$$

$$\sigma_3 = -\rho B_e (V_3 - 2V_y)$$

therefore,

$$V_3 = \frac{V_0(1 - \bar{B}^2) + V_y(8\bar{B} + 4\bar{B}^2)}{2(1 + \bar{B})^2} \quad (11)$$

and

$$\sigma_3 = -\rho B e \frac{V_0(1 - \bar{B}^2) - 2V_y}{(1 + \bar{B})^2} \quad (12)$$

Letting $\sigma_3 = -\sigma_y$ yields

$$V_0 > \frac{2V_y(3 + 2\bar{B} + \bar{B}^2)}{(1 - \bar{B})^2} \quad (13)$$

for an additional plastic wave. σ_3 can be compressive or tensile depending on the value of V_0 . When V_0 is high enough to produce an additional plastic wave, σ_3 is compressive.

The next important wave interaction is the case when the initial elastic and plastic waves in the plug and the initial elastic wave in the projectile meet at the same point in the plug. This condition is shown in Fig. 14. This interaction is solved for the V_0 region necessary to produce an additional plastic wave at point P_1 in Fig. 14 and

$$V_0 > \frac{2V_y(3 + \bar{B})}{(1 - \bar{B})} \quad (14)$$

will give an additional plastic wave.

The basic wave interactions that have been shown so far are used to solve the numerous wave interactions such as those shown in Figures 8, 11, and 14. When regions

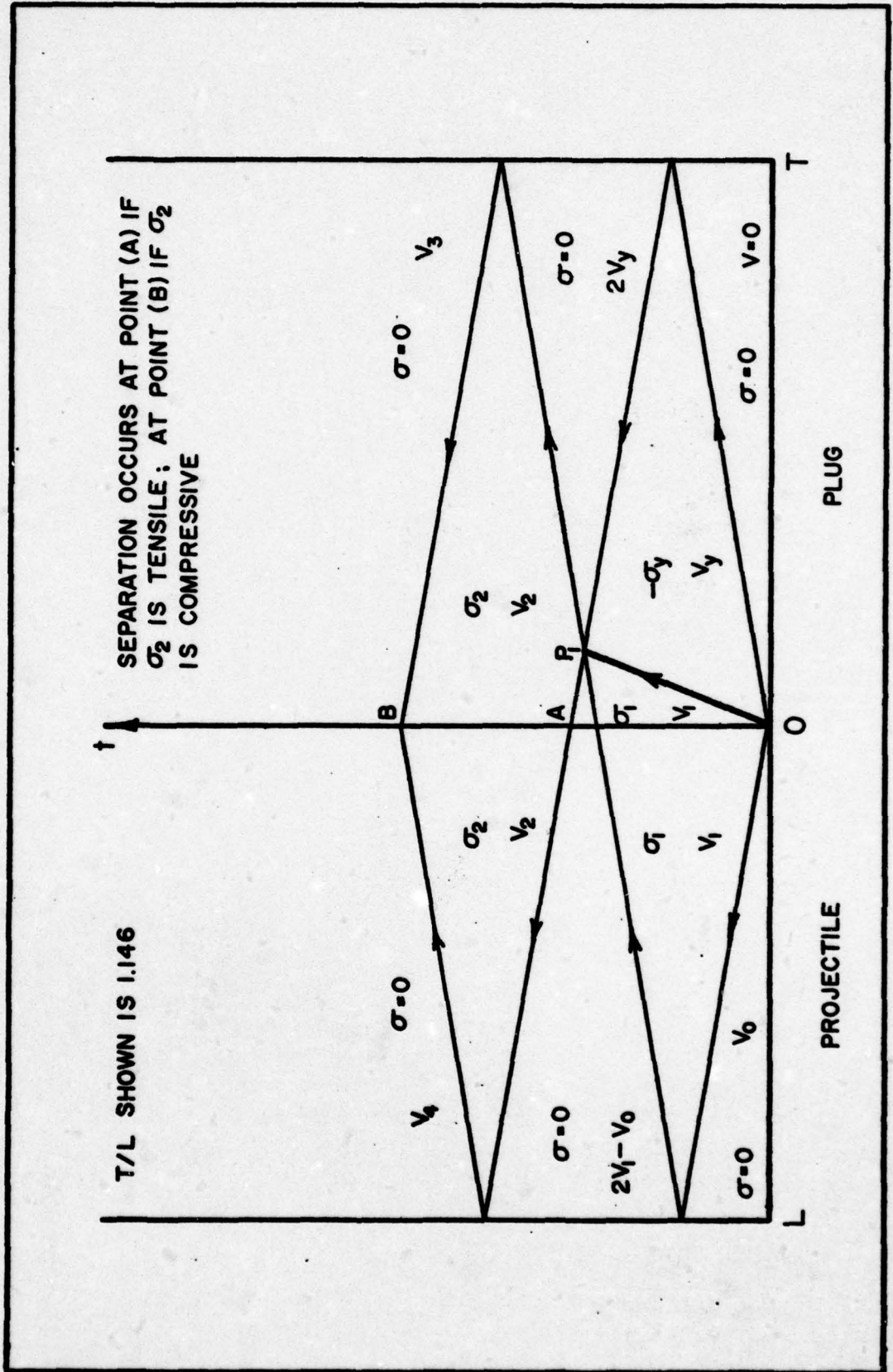


Figure 14. Simultaneous Interaction of the Three Initial Waves

where net tensile stresses reach the interface, separation takes place and the average velocity imparted to the plug is calculated. Since no additional momentum can be transferred to the plug after separation and prior to the next sub-impact, the average velocity can be calculated at any convenient time after separation. The average velocity is calculated by dividing the plate thickness into velocity regions and using

$$V_a = \frac{\sum d_i V_i}{T} \quad (15)$$

to get the average velocity, where d_i is the length of the region whose particle velocity is V_i . Since the critical initial velocity regions for subsequent plastic waves and the average velocity of the plug at any time are known, the T/L ratio is varied to locate optimum wave interactions for each of the plastic wave initial velocity regions.

Optimum Conditions

Fig. 8 shows a condition where the initial plastic wave is eliminated at point P_1 and one more elastic wave travels to the end of the plug and returns to the interface as a tensile wave. This tensile wave has a zero stress behind it and a uniform particle velocity of V_0 . If the elastic wave in the projectile enters the plug and interferes with the last tensile wave, a portion of the plug will not get accelerated to V_0 . Therefore, when the two waves meet at

the interface, separation occurs at time $2L/B_e$ and a maximum uniform particle velocity is transferred to the plug. The T/L ratio for this condition is solved for both analytically and graphically. The important feature of this interaction is the additional elastic wave that reflects from the free end of the plug and returns to the interface.

The elastic wave action is responsible for the particle velocities being imparted throughout the depth of the plug. The plastic wave serves to reflect additional elastic waves into the plug.

When the elastic wave in the projectile begins to enter the plug, a critical T/L ratio occurs when all three waves meet at the same time. This condition also allows for a maximum uniform particle velocity at separation in a minimum amount of time. The T/L ratios are solved for in the same manner as shown in Appendix D. The conditions discussed so far are limited to the initial sub-impact. Since subsequent impact velocities will be less than V_0 , it is assumed that the most effective distribution of the highest particle velocity in the shortest period of time throughout the depth of the plug will contribute the most to an optimum plugging condition. Variation of optimum conditions on subsequent sub-impacts would need to be considered for a complete analysis.

III. Results

Introduction

The previously discussed model is applied to the area of a hardened steel cylinder impacting a steel plug of 230 BHN; the results are presented as a plot of the initial projectile velocity vs. T/L ratio. The plot in Fig. 15 shows the distinct regions that result from the wave interactions. The various regions are examined and with the aid of the wave position-time diagrams, the following projectile-plug impact results are found.

Discussion

1. The stress at the interface is constant between the arrival times of successive waves at the interface. This contrasts with the rigid projectile model that resulted in an exponentially decaying stress at the interface between sub-impacts.

2. This analysis predicts separation of the projectile and plug. When $T/L < 1$ separation occurs at $2L/B_e$. This is the same separation time for two elastic cylinders. When $T/L > 1$ separation can occur at $2T/B_e$, which corresponds to the elastic case, but it may occur at a later time depending on V_0 . The wave that reaches the interface at $2T/B_e$ may be net tensile or compressive depending on V_0 . In the rigid projectile case separation occurs at $2T/B_e$ independent of V_0 or T/L .

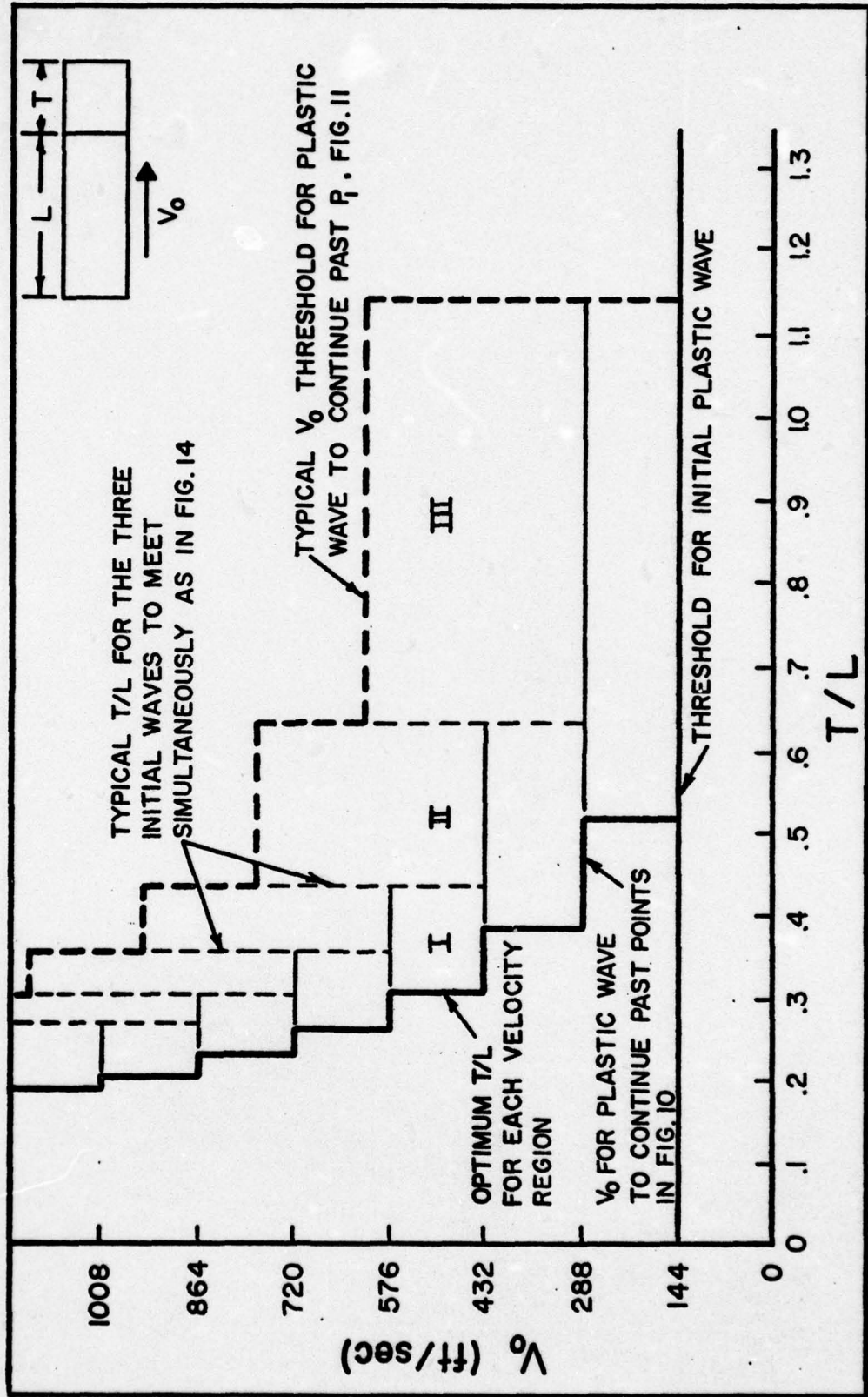


Figure 15. V_0 vs. T/L ; Optimum Conditions for Initial Impact

3. The heavy solid line in Fig. 15 represents the T/L for the optimum interaction shown in Fig. 8 for each velocity region that allows the plastic wave to continue past subsequent elastic-plastic interactions. For 230 BHN steel the minimum velocity to initiate a plastic wave is 144 ft/sec. The impact is the classical elastic case with $V_0 < 144$ ft/sec. The subsequent cases for continuation of the plastic wave are multiples of the minimum required velocity.

The T/L values on the optimum line allow the plug material beneath the projectile to be accelerated to a uniform velocity of V_0 in the least time. The region to the left of the optimum line allows a uniform velocity of V_0 in the plug, but the contact time increases.

4. Although plastic deformations are present in this model, the plug is still accelerated to a uniform velocity of V_0 for $T/L \leq (T/L)_{\text{optimum}}$. This is analogous to the elastic/elastic case for $T/L < 1$ when the target cylinder is accelerated to V_0 . In this case it occurs at an average T/L from 0.2 to 0.6 due to the plastic wave interactions.

5. For T/L to the right of the optimum line, such as region I in Fig. 15, the elastic wave in the projectile begins to interfere with the elastic wave in the plug. This reduces the amount of plug material that is accelerated to V_0 . This does not, however, change the contact time, $2L/B_e$.

If T/L is increased for a constant V_0 such as 450 ft/sec, different T/L regions will be crossed. The only effect in region I is to further reduce the amount of plug material accelerated to V_0 . When region II is entered a significant change takes place. For the plastic wave to continue past the third elastic-plastic interaction V_0 must be 784 ft/sec. For T/L less than the value at the boundary of regions I and II V_0 only has to be 576 ft/sec for the plastic wave to continue past the third elastic-plastic interaction. As region III is entered the same trend is true for the plastic wave to continue past the second elastic-plastic interaction. This increase is due to the elastic wave in the projectile interacting with the plastic wave in the plug prior to the elastic wave in the plug interacting with the plastic wave. This is basically showing that the plastic wave must be stronger to continue through two interactions with elastic tensile waves than to continue through the interaction with only one elastic tensile wave. This is shown in Fig. 11. Regions above the heavy dashed line are those where separation will occur before additional interactions can occur.

6. For T/L to the right of the heavy dashed line the contact time is not only increased, but T/L is large enough to allow multiple reflections between the plastic wave in the plug and the end of the projectile. This allows greater reduction in the plastic wave strength and makes it

easier for the reflected elastic wave in the plug to eliminate it at the first interaction. For very large T/L the number of reflections between the plastic wave and the projectile is so large that the projectile can be approximated as a rigid body.

7. Fig. 15 depicts the first sub-impact and the optimum conditions discussed are only for the first sub-impact. With reimpact occurring later, Fig. 16 shows how the regions move to the right for the subsequent sub-impacts. The third sub-impact is shown in Fig. 16. The shift to the right is due to the plastically deformed region of the plate acting elastically during the first portion of the next sub-impact. The plastic wave will be generated when the new compressive wave reaches the point where the previous plastic wave progressed as shown in Fig. 17. An elastic wave at the yield point also continues from this point. This has the effect of shortening the plug thickness. The optimum T/L line will shift to the right an amount proportional to the total plastically deformed region on the previous sub-impact. Not only do the regions shift to the right but the region between the optimum line and the heavy dashed line become larger. The fact that the shift of the optimum T/L line is to the right means that an initial T/L slightly to the right of the optimum can become optimum on a subsequent sub-impact. Therefore, better plugging conditions will exist for a T/L on or to the right of the optimum line.

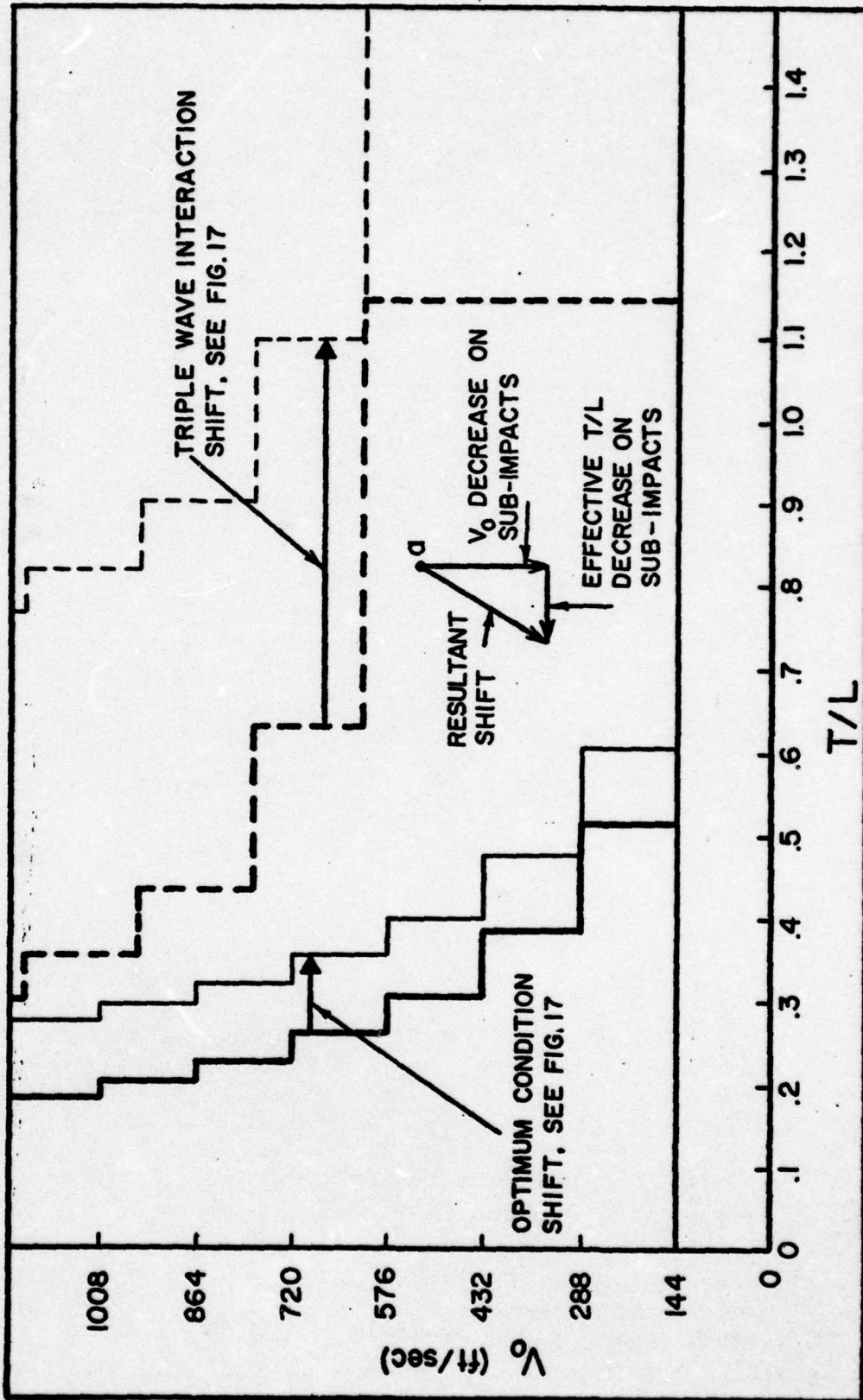


Figure 16. (T/L Shift on Third Sub-impact

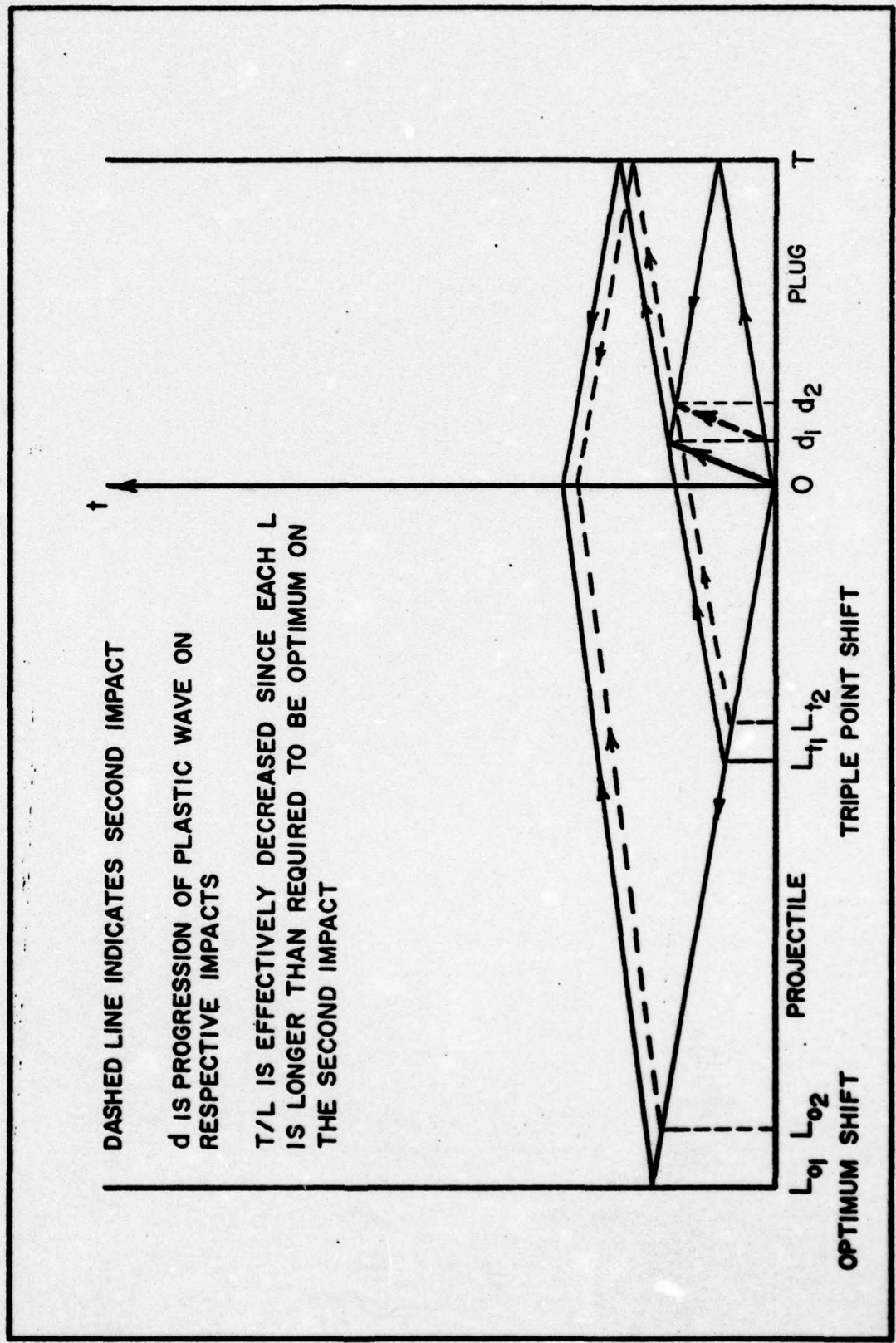


Figure 17. Delayed Plastic Wave Initiation on Second Sub-impact

Since the particle velocity for subsequent sub-impacts is reduced, V_0 may drop into a lower velocity region. This would prevent the plastic wave from continuing as far into the plug. With the optimum line shifting to the right, the effective T/L for the complete process is reduced. The combination of these two effects is shown in Fig. 16 at point (a).

8. Comparisons are made for the first sub-impact by considering the impact of two free cylinders. Figure 18 shows a plot of the normalized average velocity at separation for the elastic/elastic, rigid/elastic, and elastic/elastic-plastic cases vs. T/L. Only in the elastic/elastic-plastic case are the velocity ratios V_M/V_0 and V_m/V_0 dependent on V_0 . The two example cases selected for the elastic/elastic-plastic impact are the midpoint velocities of the first two velocity regions in Fig. 15. The higher velocity regions begin further to the left on the elastic/elastic lines where their respective optimum T/L values cross the elastic lines. Each velocity region for the elastic/elastic-plastic case follows the elastic/elastic line up to its optimum T/L. From this point the target cylinder velocity decreases linearly and the projectile velocity decreases parabolically to $T/L = 1$. From $T/L = 1$ to $T/L = 1.146$ (first triple point) the projectile velocity is constant and the target velocity decreases as $1/(T/L)$. Past the triple point the projectile velocity decreases linearly to

zero and remains zero for all higher T/L values. The target velocity decreases after the triple point as $1/(T/L)$ and becomes coincident with the $1/(T/L)$ elastic/elastic curve at the T/L where the projectile velocity becomes zero. For the second velocity region, and all higher regions, the projectile and target cylinders reach a transition point, (A), in Fig. 18, where a velocity reversal occurs. The velocity of the projectile is greater at separation than the velocity of the target from (A) to (B). At point (B) the original relative velocities are resumed. For the higher velocity regions point (A) shifts to the left and point (B) shifts to the right. The reversal region becomes larger for higher velocities. The existence of the reversal region means that the free cylinders will reimpact after separation. Although the reversal might appear to prevent separation, the interface velocity differences that result from the finite wave action cause separation. Since the plotted velocity is the average or center of mass velocity, reimpact will occur whenever the projectile has a higher velocity than the target.

The velocity reversal region is a result of the plastic wave action in the target cylinder. Equation (3) shows that the initial particle velocity in the projectile depends directly on V_0 , whereas the particle velocity in most of the target is in increments of V_y . As V_0 gets larger it exceeds the V_y increments since V_y is a constant for the

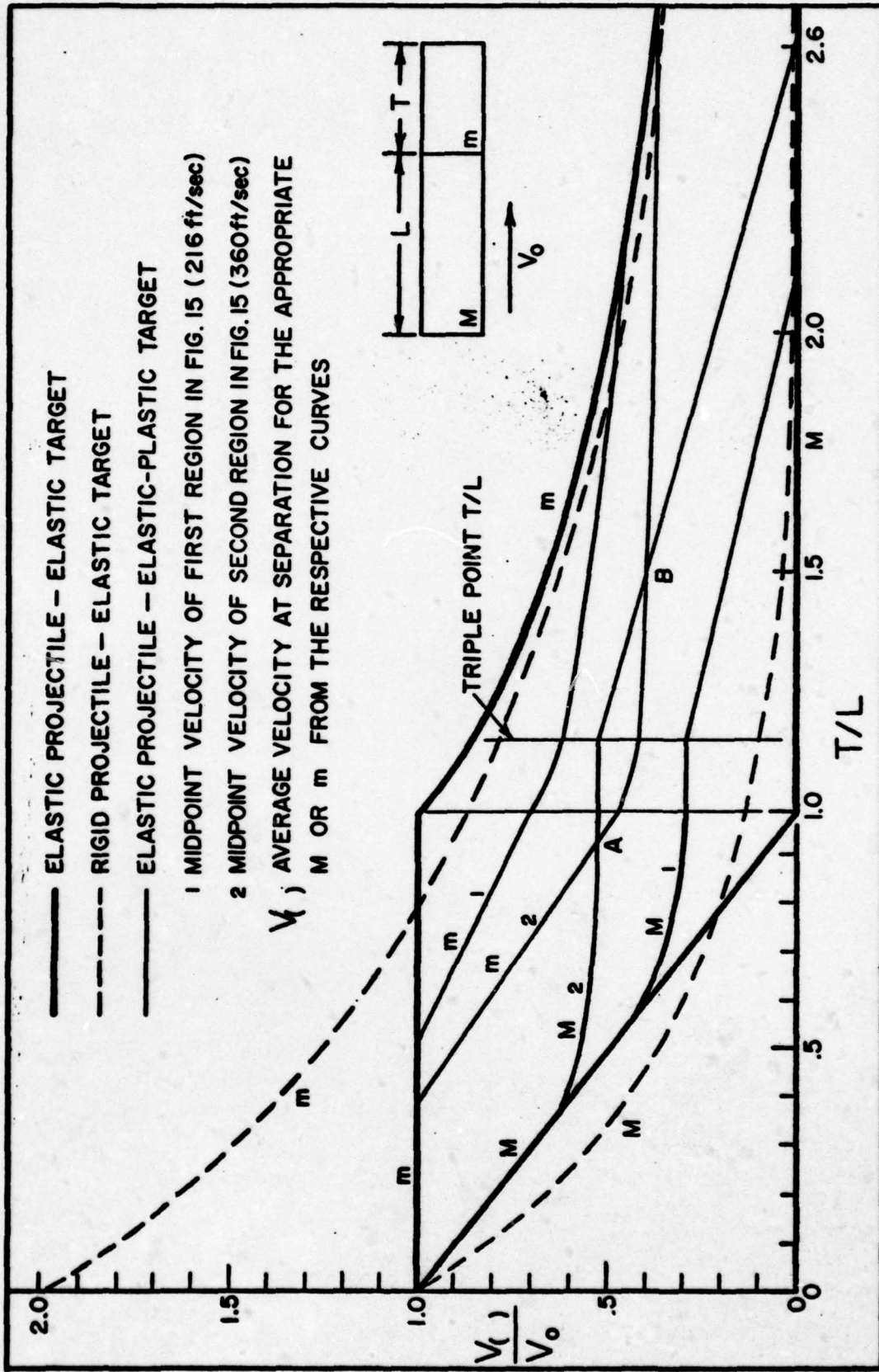


Figure 18. Comparison of Average Velocities at Separation for Free Rod Impact (Rigid Projectile Model from Ref 1)

material. The reversal begins at point (A) since the projectile will have its highest velocity at separation when $T/L < 1.146$ (first triple point). The reversal changes back at point (B) when $T/L > 1.146$ since this is where the wave in the projectile reflects numerous times between the plastic wave in the target and the free end of the projectile. Each reflection in the projectile slows the projectile until the average velocity is less than that of the target at separation. A minimum V_0 for the reversal to occur exists when points (A) and (B) coincide. This happens at $T/L = 1.146$ since this is where the target curve is lowest and the projectile curve is highest. An analytical solution for the minimum V_0 yields

$$V_0 = 308 \text{ ft/sec}$$

This velocity is approximately (within one ft/sec) the velocity for the plastic wave to continue past point P in Fig. 11. This velocity is given by

$$V_0 > \frac{4V_y}{(1-B)}$$

It is also seen that the elastic plug curve approaches the original elastic projectile curve as V approaches infinity. This reversal of velocity patterns at higher velocities is the opposite for the original elastic projectile curve as it approaches the original elastic plug curve.

IV. Application to Plate Impact

Introduction

The rod on rod impact model provides an initial condition for the plate impact problem. As shown in Fig. 2 the ejected plug is restrained within the plate by a shear force around its periphery. The state of stress jumps from pure compression/tension within the plug to pure shear at the periphery. The shear strain at the periphery increases with each increase in particle velocity caused by the compressive/tensile waves in the plug. In order for the model to result in a plugging type failure, adequate failure criteria must be established and related to the initial projectile velocity and T/L ratio.

Failure Criteria

Plugging type failures occur under conditions known as adiabatic shear failure, or thermoplastic instability. Plastic shear stresses generate large amounts of localized heating. When large stress gradients are also present, conditions exist where the rate of thermal softening can exceed the rate of work hardening. This causes an unstable condition which leads to highly localized shear strain which causes failure (Ref 6:II-40). Binkowski formulated the thermoplastic instability criteria in terms of the simple shear model used to describe plugging failures (Ref 1:58). Both approximate and exact strain solutions yield the same

condition relating shear strain, γ , at the periphery of the plug; the average velocity imparted to the plug, V_a ; and the plastic shear wave velocity, B . The relationship is

$$\gamma = \frac{V_a}{B}$$

Binkowski also showed that there is a critical shear strain for failure to occur and this critical value is a material property. This implies that a critical average particle velocity must be imparted to the plate material for failure to occur. This further implies that conditions causing maximum particle velocities to be imparted during each sub-impact optimize the plugging process. The problem becomes one of determining optimum velocity loading conditions under the influence of both elastic and plastic wave action.

Discussion

1. Plugging type failures require small outer plate deformations. The developed model predicts separation of the projectile and plate, thus keeping the contact time short and the momentum transferred to the outer plate material a minimum.

2. Binkowski (Ref 1) showed that the first two sub-impacts have the largest affect in plugging failures. Therefore, the optimum rod on rod conditions shown in Fig. 15 are significant in the plate impact problem since they

are valid for the initial impact. . Since the initial projectile velocity determines the duration of the plastic wave in the plate and hence the number of elastic reflections through the depth of the plate, it is expected to have the largest effect on the failure conditions.

3. The decrease in optimum (T/L) with increasing initial velocity applies to all subsequent sub-impacts. The T/L values on the optimum line allow the plate material beneath the projectile to be accelerated to a uniform velocity of V_0 when the projectile and plate have the same density and the same elastic wave velocity.

4. The velocity reversal region shown in Fig. 18 significantly affects the complete plate failure problem. Since the reimpact of free rods in this region is superimposed on the reimpact due to the retarding effect of the outer plate material, a very complex condition exists. The analysis of subsequent reimpact velocities is not as straightforward as when the reimpact is only caused by the retarding effect of the outer plate material. The effect of the velocity reversal region can be fully explained when exact velocities and displacements are tracked at the interface during separation. This will give exact reimpact velocities due to both reimpact mechanisms.

5. Projectile design problems can be approached by the use of this model. If fragment sizes and target thicknesses are known and projectile to target distance is fixed, the

velocity required to penetrate the target can be determined from a plot such as Fig. 15. Knowing the required velocity would determine the explosive charge size and hence affect the weight of the weapon. Any of the variables T , L , or V_0 can be specified when the other two are known. An analytical model that provides a good first guess can save testing time and money.

6. A comparison with experimental failure curves (Ref 2) can only be done qualitatively since the sub-impact velocities are not known. However, the optimum (T/L) shift is known and the initial projectile velocity is a maximum with respect to the sub-impact velocities. Figure 19 shows the initial and third sub-impact optimum lines compared to an experimental plate failure curve. The initial velocity values for the experimental curve are those required to cause plate failure. Figure 19 shows the experimental dishing region to the left of the initial impact optimum line. This is where the model predicts conditions for dishing type failures. When additional sub-impacts are considered, the heavy dashed boundary moves to the right enough to let the experimental penetration region fall to the right of the boundary. This leaves the experimental plugging region in the middle where the model shows plugging conditions to be more favorable. This is not an exact correlation in view of the scatter in the experimental data and the transitions that exist between the three modes of plate perforation.

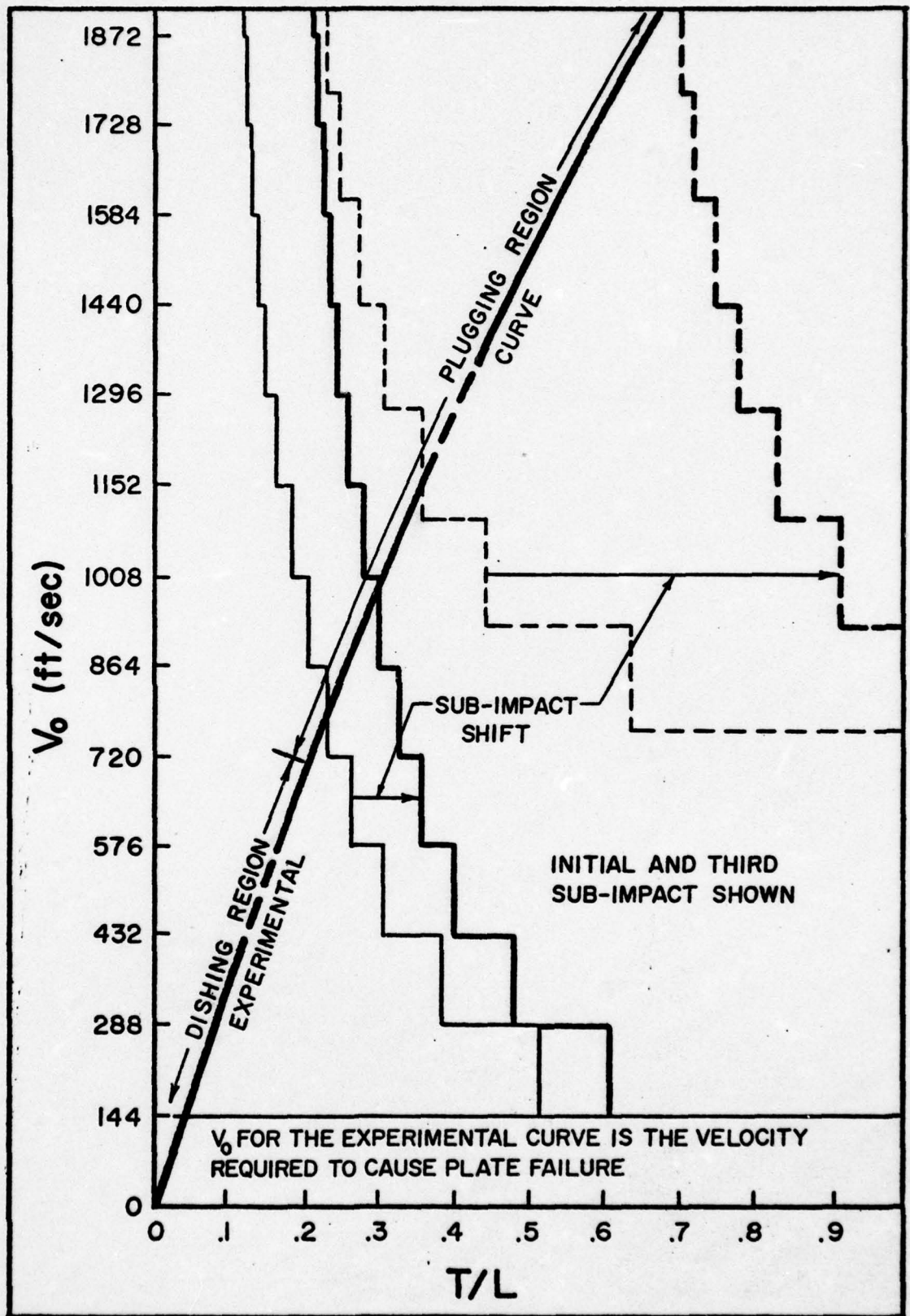


Figure 19. Comparison With Experimental Failure Data (Failure Data from Ref 2)

7. Due to the plastic wave action, the initial contact time has an upper limit independent of V_0 . This limit is the travel time of the plastic wave through the plug thickness, T/B_p . This is seen graphically in Fig. 10 as the time when the heavy solid plastic curve intersects the vertical line at thickness T . Although this maximum contact time will never be approached by ballistic velocities, it would be of interest to high velocity impact problems.

V. Recommendations

1. This model should be applied to a steel projectile impacting an aluminum plate. The primary difference will occur in the stress equations due to the density difference and the wave velocity difference.

2. Since the model shows that the elastic-plastic wave interactions can be approached in a systematic manner, a computer model should be developed to ease the computational rigor of the wave interactions. Computerized solutions of the wave position-time diagrams would be extremely useful in analyzing the values of the optimum T/L ratios at higher ballistic velocities. The graphical plots are essential to tracking the internal wave interactions as well as providing a better understanding of the impact problem.

3. Experimental studies should be done to verify the plastic wave penetration in the ejected plug. Microscopic analysis of specimens could be compared to the analytical predictions at specified initial velocities and T/L ratios. This would provide an excellent validation of the elastic/elastic-plastic model.

4. This model should be extended to include all sub-impacts to failure as determined by the critical shear strain value. This would allow comparison with experimental ballistic limit velocities and also with the rigid projectile model. With the complete process modeled, the effect of the velocity reversal region can be completely explored.

Bibliography

1. Binkowski, R. D. The Deformation and Failure of Plates Due to Impact by Blunt Rigid Projectiles. Unpublished Dissertation. Denver, Colorado: University of Denver, May 1975.
2. Hoggart, C. R. and R. F. Recht. "Stress-Strain Data Obtained at High Rates Using an Expanding Ring." Experimental Mechanics, Vol. 9: p. 441 (1969).
3. Chou, P. C. and A. K. Hopkins. Dynamic Response of Materials to Intense Impulsive Loading. Dayton: Air Force Materials Laboratory, 1972.
4. Goldsmith, W. Impact. Landon: Edward Arnold (Publishers) Ltd., 1960.
5. Kolsky, H. Stress Waves in Solids. Oxford: Clarendon Press, 1953.
6. Recht, R. F. Dynamic Deformation of Metals as Related to High-Energy Rate Forming. Denver: Martin Company, Denver Division; Part II, First Annual Report, Center for High Energy Forming, 1966.

Appendix A

Initial Impact Solution

Figure A-1 is used to write the momentum balance equation across the left traveling elastic wave and the right traveling plastic wave. When this is done, two equations

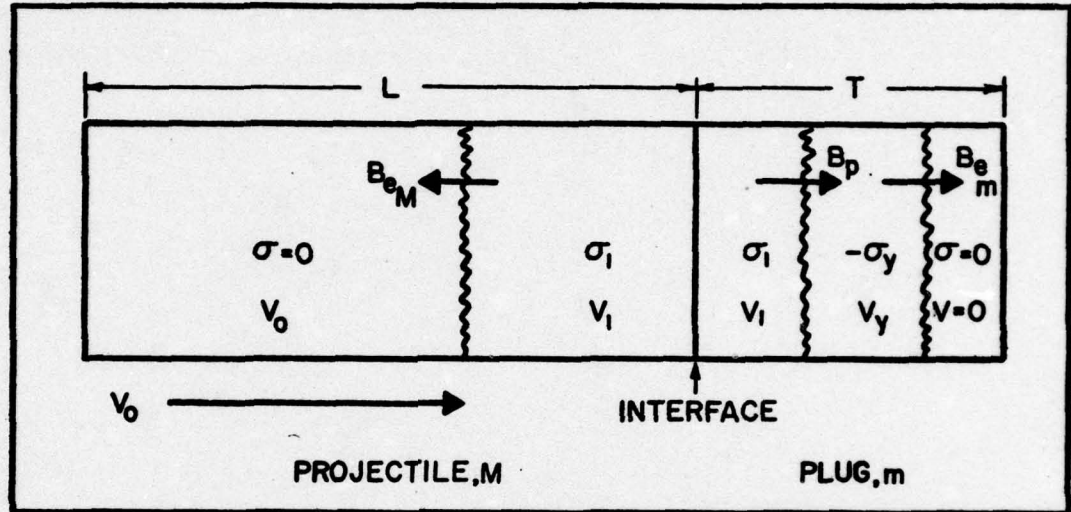


Figure A-1. Initial Impact Wave Relationships

for the two unknowns σ_1 and v_1 are obtained. They are

$$\sigma_1 = -\rho_M B_{eM} (v_0 - v_1)$$

$$\sigma_1 = -\rho_m B_{em} v_y - \rho_m B_p (v_1 - v_y)$$

The second equation is rewritten

$$\begin{aligned} \sigma_1 &= -\sigma_y - \rho_m B_p v_1 + \rho_m B_p v_y \\ &= -\sigma_y - \rho_m B_p v_1 + \rho_m B_{em} v_y \frac{B_p}{B_{em}} \\ &= -\sigma_y \left(1 - \frac{B_p}{B_{em}}\right) - \rho_m B_p v_1 \end{aligned}$$

Setting the two equations equal

$$-\rho_M B_{eM} V_0 + \rho_M B_{eM} V_1 = -\sigma_y \left(1 - \frac{B_p}{B_{em}}\right) + \rho_m B_p V_1$$

They are solved for v_1 yielding

$$V_1 = \frac{\rho_M B_{eM} V_0 - \sigma_y \left(1 - \frac{B_p}{B_{em}}\right)}{(\rho_M B_{eM} + \rho_m B_p)}$$

When $\rho_m = \rho_M = \rho$ and $B_{em} = B_{eM} = B_e$

$$V_1 = \frac{V_0 - V_y (1 - \bar{B})}{(1 + \bar{B})} \quad (1)$$

where $\bar{B} = \frac{B_p}{B_e}$

Substituting v_1 back into one of the original equations

$$\begin{aligned} \sigma_1 &= -\rho_M B_{eM} (V_0 - V_1) \\ &= -\rho_M B_{eM} V_0 + \rho_M B_{eM} V_1 \end{aligned}$$

$$\sigma_1 = \frac{-\rho_M B_{eM} V_0 \left(1 + \frac{\rho_m B_p}{\rho_M B_{eM}}\right) + \rho_M B_{eM} \left[V_0 - \frac{\rho_m}{\rho_M} \left(\frac{B_{em}}{B_{eM}} - \frac{B_p}{B_{em}}\right) V_y\right]}{1 + \frac{\rho_m B_p}{\rho_M B_{eM}}}$$

After simplifying

$$\sigma_1 = \frac{-\left[\rho_M B_p V_0 + \sigma_y \left(1 - \frac{B_p}{B_{em}} \right) \right]}{1 + \frac{\rho_m}{\rho_M} \frac{B_p}{B_{eM}}}$$

When $\rho_m = \rho_M = \rho$ and $B_{em} = B_{eM} = B_e$

$$\sigma_1 = \frac{-\left[\rho B_p V_0 + \sigma_y (1 - \bar{B}) \right]}{(1 + \bar{B})} \quad (2)$$

Appendix B

First Elastic-Plastic Wave Interaction Resulting
In a Continuation of the Plastic Wave

Figure B-1b is used to write the momentum balance equation across the left traveling elastic wave and the right traveling plastic wave as they leave the point of interaction.

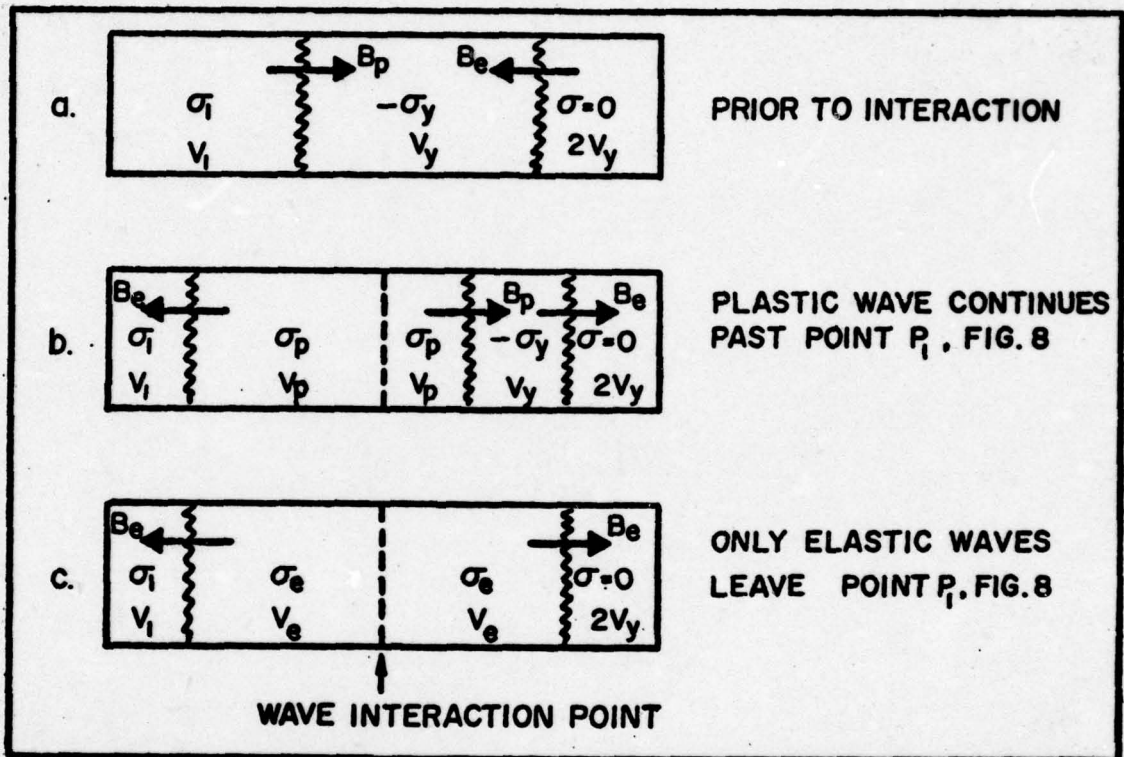


Figure B-1. Initial Elastic-Plastic Wave Interaction

When this is done, two equations for the two unknowns v_p and σ_p are obtained. They are

$$\sigma_p = \sigma_1 + \rho B_e (v_p - v_1)$$

$$\sigma_p = -\sigma_y - \rho B_p (v_p - 3v_y)$$

It is seen that the stress history of each point is carried on through its particle velocity at any given time.

The momentum equations are solved simultaneously for V_p , yielding

$$\sigma_1 + \rho B_e (V_p - V_1) = -\sigma_y - \rho B_p (V_p - 3V_y)$$

$$V_p = \frac{V_1 - V_y(1 - 3\bar{B}) - \frac{\sigma_1}{\rho B_e}}{(1 + \bar{B})} \quad (1)$$

where $\bar{B} = \frac{B_p}{B_e}$

After substituting in V_1 and σ_1 from Appendix A and simplifying

$$V_p = \frac{V_0 - V_y(1 - 3\bar{B})}{(1 + \bar{B})} \quad (2)$$

Comparing equation (2) with equation (1), it is seen that

$$V_0 = V_1 - \frac{\sigma_1}{\rho B_e} \quad (3)$$

from a comparison of the numerator terms. Substituting σ_1 and V_1 into equation (3) verifies that equation (2) is correct.

Substituting equation (2) back into either original momentum equation gives

$$\sigma_p = -\rho B_e \left[\frac{V_0 \bar{B} + V_y (1 - 3\bar{B})}{(1 + \bar{B})} \right] \quad (4)$$

In order to determine the limiting value of V_0 that will prevent the plastic wave from continuing past the first elastic-plastic interaction, a momentum balance is written using Fig. B-1c. The momentum balance yields

$$\sigma_e = \sigma_i + \rho B_e (V_e - V_i)$$

$$\sigma_e = -\rho B_e (V_e - 2V_y)$$

Setting these equal yields

$$\sigma_i + \rho B_e (V_e - V_i) = -\rho B_e (V_e - 2V_y)$$

$$\frac{\sigma_i}{\rho B_e} + V_e - V_i = -V_e + 2V_y$$

and

$$V_e = V_y + \frac{1}{2} V_i - \frac{\sigma_i}{2\rho B_e}$$

Substituting in V_i and σ_i yields

$$V_e = \frac{1}{2} V_0 + V_y \quad (5)$$

Substituting back into the momentum equation yields

$$\sigma_e = -\rho B_e \left(\frac{1}{2} V_0 - V_y \right) \quad (6)$$

To find the limiting V_0 equation (6) is set equal to $-\sigma_y$ yielding

$$-\sigma_y = -\rho B_e V_y = -\rho B_e \frac{1}{2} V_0 - V_y$$

or

$$V_y = \frac{1}{2} V_0 - V_y$$

and

$$V_{0 \text{ crit}} = 4V_y$$

V_y is the particle velocity jump across a stress wave at the yield point. For 230 BHN steel

$$V_y = 72 \text{ ft/sec}$$

and

$$V_{0 \text{ crit}} = 288 \text{ ft/sec}$$

When successive interactions are solved they are found to be multiples of the V_0 necessary to have an initial plastic wave, namely

$$V_{0 \text{ crit}} = 2V_y = 144 \text{ ft/sec}$$

Appendix C

Plastic-Unloading Wave Interaction

Figure C-1 is used to write the momentum balance equation across the left traveling elastic wave and the right traveling plastic wave. This case assumes that the unloading wave does not eliminate the original plastic wave.

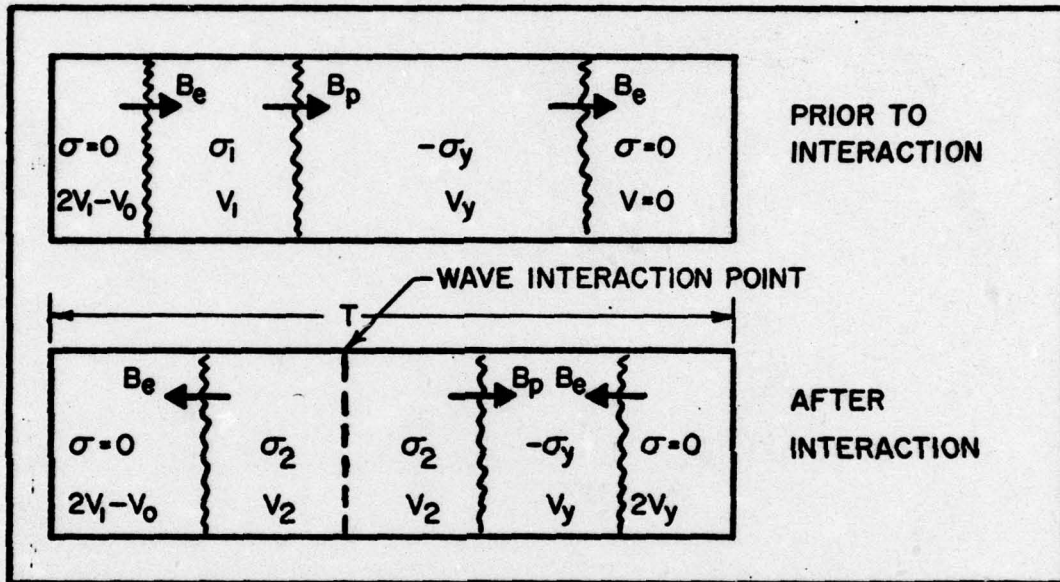


Figure C-1. Plastic-Unloading Wave Interaction

When this is done, two equations for the two unknowns V_2 and σ_2 are obtained. They are

$$\sigma_2 = \rho B_e (V_2 - 2V_1 + V_0)$$

$$\sigma_2 = -\sigma_y - \rho B_p (V_2 - V_y)$$

These two are solved simultaneously for V_2 yielding

$$V_2 = \frac{2V_1 - V_0 - V_y(1 - \bar{B})}{(1 + \bar{B})}$$

Substituting in for V_1 from Appendix A and simplifying, V_2 becomes

$$V_2 = \frac{V_0(1 - \bar{B}) - V_y(3 - 2\bar{B} - \bar{B}^2)}{(1 + \bar{B})^2} \quad (1)$$

Substituting back into the momentum equation σ_2 is solved for yielding

$$\sigma_2 = -\rho B_e \left[\frac{V_0(\bar{B} - \bar{B}^2) + V_y(1 - 2\bar{B} + \bar{B}^2)}{(1 + \bar{B})^2} \right] \quad (2)$$

When this reduced plastic wave meets the initial elastic wave at point P_1 in Fig. 11, it is assumed that the plastic wave is eliminated and the resulting equations are used to solve for the limiting V_0 for this condition. Balancing momentum yields

$$\sigma_3 = \sigma_2 + \rho B_e (V_3 - V_2)$$

$$\sigma_3 = -\rho B_e (V_3 - 2V_y)$$

These are solved simultaneously for V_3 yielding

$$V_3 = V_y + \frac{1}{2} V_2 - \frac{\sigma_2}{2\rho B_e}$$

The interactions are successively more complex with each interaction since the particle velocities reflect the previous stress time history.

Substituting for V_2 and σ_2 yields

$$V_3 = \frac{V_0(1-\bar{B}^2) + V_y(8\bar{B} + 4\bar{B}^2)}{2(1+\bar{B})^2} \quad (3)$$

and

$$\sigma_3 = -\rho B_e \left[\frac{\frac{1}{2} V_0(1-\bar{B}^2) - 2V_y}{(1+\bar{B})^2} \right] \quad (4)$$

The limiting V_0 to eliminate the plastic wave is found by setting

$$\sigma_3 = -\sigma_y$$

This yields

$$V_{o_{crit}} = \frac{2V_y (3 + 2\bar{B} + \bar{B}^2)}{(1 + \bar{B})^2} \quad (5)$$

For 230 BHN steel

$$V_{o_{crit}} = 452 \text{ ft/sec}$$

This is the case when $T/L > 1.146$, which is not of primary interest for plugging type plate failures.

When the same procedure is used in the region above point P_1 in Fig. 11, a limiting velocity is found for $.63 < T/L < 1.146$. This solution yields

$$V_{o_{crit}} = 618 \text{ ft/sec}$$

which is the value of the horizontal heavy dashed line for $.63 < T/L < 1.146$. The successive steps in this process are found to be increments of 166 ft/sec starting with 452 ft/sec.

Appendix D
Critical T/L Solutions

Analytical

The critical T/L values are found by establishing the wave interaction points that allow the plug to be uniformly the same velocity without interference from the wave in the projectile. The equations are written by setting the time of travel for both waves equal and solving for the required T/L. This is done for the successive interactions shown in Fig. 10.

Figure D-1 shows the condition where the plastic wave is eliminated at the second interaction with the reflected elastic tensile wave. The distance to the point where the plastic wave meets the initial reflected wave is d_m . If the plastic wave continues to d'_m and is eliminated at that

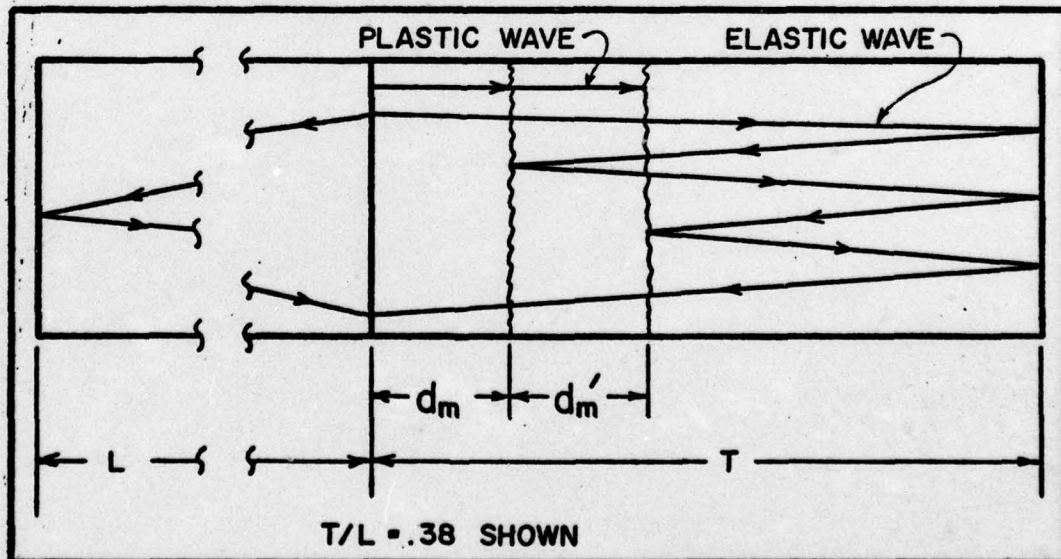


Figure D-1. Analytic Solution for T/L Critical

point, the elastic wave makes one more trip to the free end of the plug and then returns to the interface with a uniform velocity of V_0 behind it. The optimum condition exists when the projectile is long enough to allow its elastic wave to meet the final elastic wave in the plug at the interface.

The time for the initial plastic wave to travel d_m is

$$t_p = \frac{d_m}{B_e}$$

In the same time the initial elastic wave travels a distance

$$(2T - d_m)$$

in a time

$$t_e = \frac{2T - d_m}{B_e}$$

Setting the times equal yields

$$d_m = \frac{2B_p T}{B_e + B_p} \quad (1)$$

The time for the second plastic wave to travel d'_m is

$$t_p = \frac{d'_m}{B_e}$$

In the same time the elastic wave travels

$$\left[2(T - d_m) - d'_m \right]$$

in a time

$$t_e = \frac{2(T - d_m) - d'_m}{B_e}$$

Setting the times equal yields

$$d'_m = \frac{2TB_p(B_e - B_p)}{(B_e + B_p)} \quad (2)$$

The total distance the elastic wave travels to return to the interface is

$$d = 6T - 4d_m - 2d'_m$$

After substituting for d_m and d'_m

$$d = \frac{2T(3B_e^2 + B_p^2)}{(B_e + B_p)^2}$$

The time to travel this distance is

$$t_e = \frac{d}{B_e}$$

The time of travel for the wave in the projectile to reach the interface is

$$t_e = \frac{2L}{B_e}$$

Setting the times equal yields

$$\frac{2T(3B_e^2 + B_p^2)}{B_e(B_e + B_p)^2} = \frac{2L}{B_e}$$

which results in

$$\left(\frac{T}{L}\right)_{\text{crit}} = \frac{B_e + B_p}{(3B_e^2 + B_p^2)}$$

For 230 BHN steel and the projectile and plug the same material

$$\left(\frac{T}{L}\right)_{\text{crit}} = .38$$

This method was used for the first three T/L conditions and the complexity of the equations increased rapidly. Using the first three points as a check, a graphical method was used to solve for successive points.

Graphical Method

The graphical time-position plots were developed by assuming an elastic wave angle and using the first analytical solution for T/L at the triple point (where all three waves meet) to establish the plastic wave angle.

Since the actual angles are very small, 10° was selected for the elastic wave angle. The distance L was determined from the analytic T/L solutions, T being arbitrarily

fixed. The condition that all three waves meet at one point determines the unknown plastic wave angle relative to the elastic angle as shown in Fig. D-2. In this case the plastic angle is 68° . Once this is determined additional wave interactions can be drawn and the required L found for a fixed T . Points past the third critical point were found in this manner.

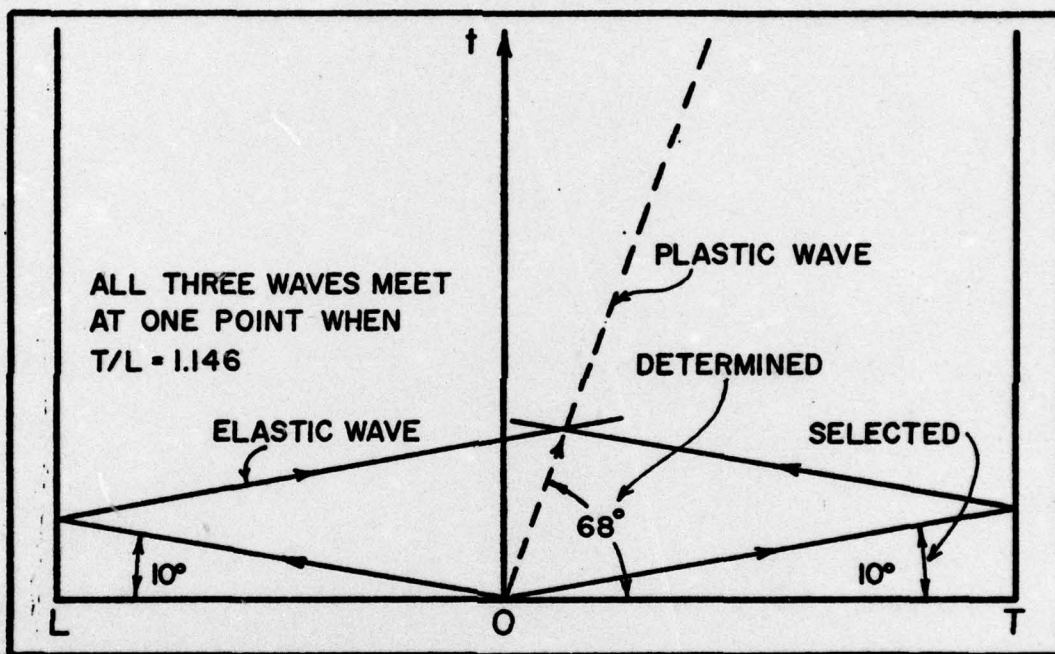


Figure D-2. Graphical Solution for T/L Critical

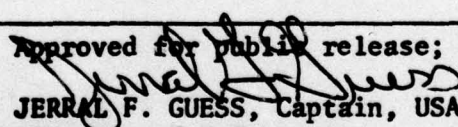
Vita

Kenneth C. Leone was born on 17 October 1943 in Wilmington, Delaware. He attended the University of Kansas where he served as Chairman of the Student Branch of the American Institute of Aeronautics and Astronautics. In February 1967 he received his Bachelor of Science degree in Aerospace Engineering and his commission in the United States Air Force. Upon graduation he worked for six months as a structural design engineer for McDonnell-Douglas Aircraft Corporation, St. Louis, Missouri. In July 1967 he was assigned to Undergraduate Pilot Training at Moody AFB, Georgia. Upon graduation from pilot training in January 1969, he attended survival school and was assigned to the 316 Tactical Airlift Wing at Langley AFB, Virginia as a C-130E co-pilot. In December 1970 he was assigned to the 16 Special Operation Squadron in Ubon, Thailand as a AC-130A Gunship co-pilot. For the last three months of his Southeast Asia tour he was assigned to the 834 Air Division at Tan Son Nhut A.B., Vietnam where he served in the airfield survey office. He then returned to the 316 Tactical Airlift Wing in December, 1971 where he served as a C-130E instructor pilot, squadron flight commander, and finally as officer in charge of the C-130E Flight Simulator. He reported in May 1975 to the Air Force Institute of Technology (AFIT) where he enrolled in the Graduate Aeronautical Engineering (structures option) program.

His permanent address is 35 Kehoe Street, Clifton,
New Jersey 07011.

UNCLASSIFIED

SECURITY CLASSIFICATION OF THIS PAGE (When Data Entered)

REPORT DOCUMENTATION PAGE		READ INSTRUCTIONS BEFORE COMPLETING FORM
1. REPORT NUMBER GAE/MC/76D-4	2. GOVT ACCESSION NO.	3. RECIPIENT'S CATALOG NUMBER
4. TITLE (and Subtitle) Ballistic Impact Between a Blunt Elastic Projectile and An Elastic-Plastic Plate		5. TYPE OF REPORT & PERIOD COVERED MS Thesis
7. AUTHOR(s) Kenneth C. Leone Capt, USAF		6. PERFORMING ORG. REPORT NUMBER
9. PERFORMING ORGANIZATION NAME AND ADDRESS Air Force Institute of Technology (AFIT-EN) Wright-Patterson AFB, Ohio 45433		8. CONTRACT OR GRANT NUMBER(s)
11. CONTROLLING OFFICE NAME AND ADDRESS		10. PROGRAM ELEMENT, PROJECT, TASK AREA & WORK UNIT NUMBERS
14. MONITORING AGENCY NAME & ADDRESS (if different from Controlling Office)		12. REPORT DATE December, 1976
		13. NUMBER OF PAGES 77
		15. SECURITY CLASS. (of this report) Unclassified
16. DISTRIBUTION STATEMENT (of this Report)		15a. DECLASSIFICATION/DOWNGRADING SCHEDULE
<div style="border: 1px solid black; padding: 5px; display: inline-block;"> DISTRIBUTION STATEMENT A Approved for public release; Distribution Unlimited </div>		
17. DISTRIBUTION STATEMENT (of the abstract entered in Block 20, if different from Report) Approved for public release; distribution unlimited.		
18. SUPPLEMENTARY NOTES Approved for public release; IAW AFR 190-17 <div style="text-align: center;">  JERRAL F. GUESS, Captain, USAF Director of Information </div>		
19. KEY WORDS (Continue on reverse side if necessary and identify by block number) Ballistic Impact Blunt Projectile Plate Impact Elastic Impact Plastic Impact		
20. ABSTRACT (Continue on reverse side if necessary and identify by block number) A cylindrical rod on rod impact model is developed that allows for linear elastic strains in the projectile and linear elastic-plastic strains in the target plug. Application is made to the plate impact problem. Normal incidence impact of two circular cylinders is considered. One-dimensional stress waves load the projectile and the plug		

UNCLASSIFIED

SECURITY CLASSIFICATION OF THIS PAGE (When Data Entered)

Block 20.

→ in compression and tension. Stress wave interactions are tracked in the projectile and in the plug. Momentum balance is used to solve for resultant stresses and particle velocities. Optimum conditions are determined for the initial impact that allow the plug to be accelerated uniformly to the initial projectile velocity. Optimum plug length/projectile length ratio is found to decrease with increasing projectile initial velocity. Separation of the projectile and plug is predicted and separation times are determined. ← Average velocities at separation are determined and plotted vs. plug length/projectile length ratio. A comparison is made on this plot with the elastic/elastic and the rigid/elastic free rod cases. A velocity reversal region is identified, where the average projectile velocity is greater than the average plug velocity at separation, which causes the free rods to reimpact. The model provides an initial condition for the plate impact problem. The optimum plate thickness/projectile length ratio increases on subsequent sub-impacts. Qualitative extensions indicate optimum plugging conditions. The model suggests that for thin plates the plate material is accelerated to the initial projectile velocity. It also suggests that projectiles are essentially rigid for thick plate impacts as long as the projectile does not deform plastically.